TOPICAL REVIEW • OPEN ACCESS

Fundamentals of hydrogen storage in nanoporous materials

IOP Publishing Prog. Energy 4 (2022) 042013 https://doi.org/10.1088/2516-1083/ac8d44

Progress in Energy

OPEN ACCESS

RECEIVED
12 May 2022

REVISED
15 August 2022

ACCEPTED FOR PUBLICATION
26 August 2022

PUBLISHED
14 September 2022

TOPICAL REVIEW

Fundamentals of hydrogen storage in nanoporous materials

Linda Zhang[1], Mark D Allendorf[2], Rafael Balderas-Xicohténcatl[1,3], Darren P Broom[4], George S Fanourgakis[5], George E Froudakis[5], Thomas Gennett[6,7], Katherine E Hurst[6], Sanliang Ling[8], Chiara Milanese[9], Philip A Parilla[6], Daniele Pontiroli[10], Mauro Riccò[10], Sarah Shulda[6], Vitalie Stavila[2], Theodore A Steriotis[11], Colin J Webb[12], Matthew Witman[2] and Michael Hirscher[1,*]

[1] Max-Planck-Institut für Intelligente Systeme, Heisenbergstrasse 3, 70569 Stuttgart, Germany
[2] Sandia National Laboratories, Livermore, CA 94551, United States of America
[3] Neutron Scattering Division, Neutron Sciences Directorate, Oak Ridge National Laboratory, Oak Ridge, TN 37831, United States of America
[4] Hiden Isochema, 422 Europa Boulevard, Warrington WA5 7TS, United Kingdom
[5] Department of Chemistry, University of Crete, Voutes Campus, GR-70013 Heraklion, Crete, Greece
[6] National Renewable Energy Laboratory, Golden, CO 80401, United States of America
[7] Department of Chemistry, Colorado School of Mines, Golden, CO 80401, United States of America
[8] Advanced Materials Research Group, Faculty of Engineering, University of Nottingham, University Park, Nottingham NG7 2RD, United Kingdom
[9] Pavia Hydrogen Lab, Chemistry Department, Physical Chemistry Section, University of Pavia and C.S.G.I., Viale Taramelli 16, I-27100 Pavia, Italy
[10] Nanocarbon Laboratory, Dipartimento di Scienze Matematiche, Fisiche e Informatiche, Università di Parma, Parco Area delle Scienze, 7/a, I-43124 Parma, Italy
[11] National Center for Scientific Research 'Demokritos', 15341 Ag. ParaskeviAttikis, Athens, Greece
[12] Queensland Micro- and Nanotechnology Centre, Griffith University, Brisbane, QLD 4111, Australia
* Author to whom any correspondence should be addressed.

E-mail: hirscher@is.mpg.de

Keywords: energy storage, porous materials, adsorption, machine learning

Abstract

Physisorption of hydrogen in nanoporous materials offers an efficient and competitive alternative for hydrogen storage. At low temperatures (e.g. 77 K) and moderate pressures (below 100 bar) molecular H_2 adsorbs reversibly, with very fast kinetics, at high density on the inner surfaces of materials such as zeolites, activated carbons and metal–organic frameworks (MOFs). This review, by experts of Task 40 'Energy Storage and Conversion based on Hydrogen' of the Hydrogen Technology Collaboration Programme of the International Energy Agency, covers the fundamentals of H_2 adsorption in nanoporous materials and assessment of their storage performance. The discussion includes recent work on H_2 adsorption at both low temperature and high pressure, new findings on the assessment of the hydrogen storage performance of materials, the correlation of volumetric and gravimetric H_2 storage capacities, usable capacity, and optimum operating temperature. The application of neutron scattering as an ideal tool for characterising H_2 adsorption is summarised and state-of-the-art computational methods, such as machine learning, are considered for the discovery of new MOFs for H_2 storage applications, as well as the modelling of flexible porous networks for optimised H_2 delivery. The discussion focuses moreover on additional important issues, such as sustainable materials synthesis and improved reproducibility of experimental H_2 adsorption isotherm data by interlaboratory exercises and reference materials.

1. Introduction

Developing a safe, affordable and efficient way of storing H_2 is a key priority in hydrogen energy research. Current fuel cell vehicles, such as the Toyota Mirai, use 700 bar compressed H_2, which provides a gravimetric H_2 capacity of approximately 5.7 wt% and a volumetric capacity of 40 g H_2 l^{-1} [1]. Compressed H_2 storage offers quick refill times and provides long ranges for fuel cell vehicles, but it also has some disadvantages. Compressing H_2 to 700 bar, for example, consumes energy, and further gains in volumetric and gravimetric

capacity can only be achieved by using yet higher pressures. The need for high pressures limits tank shape to non-conformable carbon fibre-reinforced composite cylinders, which are also expensive, while isenthalpic expansion of H_2 during charging leads to temperature increases, so H_2 must be pre-cooled to 233 K to avoid overheating [2]. H_2 can also be stored as a liquid, but this requires very low temperatures, below 30 K [3, 4]. Cooling H_2 to this extent consumes more energy than 700 bar compression and long-term storage requires highly insulated tanks, which are, again, rather expensive. A third option, known as *cryo-compression*, combines cooling and compression, to achieve high volumetric densities close to liquid H_2 in the gaseous state [5, 6].

A general alternative to storing H_2 in compressed, liquid or cryo-compressed form is to use materials that absorb or adsorb hydrogen, to provide high gravimetric and volumetric capacities at more practical pressures and temperatures [7, 8]. Various options exist, as discussed throughout this special issue, but each one has disadvantages, as well as advantages. Metal and complex hydrides bind hydrogen in their structure, and can therefore be categorised as a form of chemical hydrogen storage [4]. Complex hydrides can provide high gravimetric and volumetric capacities, but they are not always reversible, often require high temperatures for operation, and, when reversible, usually have sluggish hydrogen absorption and desorption kinetics. Interstitial metal hydrides that can operate at near ambient temperature, meanwhile, can possess impressive volumetric capacities, exceeding that of liquid H_2 [9], but they usually exhibit low gravimetric capacities, below 2 wt%. Moreover, in all cases, since hydrogen is chemically bound via ionic, metallic or covalent bonds, the respective sorption and desorption enthalpies are considerable, and heat management then becomes a key issue for optimal operation [10].

Hydrogen adsorption in nanoporous materials is an alternative physical, rather than chemical, solution to the hydrogen storage problem [4]. In this case, molecular H_2 is physically adsorbed, or *physisorbed*, in the pores of materials with very high internal surface areas and hence extended gas–solid interfaces, such as zeolites [11], activated carbons, and metal–organic frameworks (MOFs) [12–16]. Using this approach, H_2 can be stored at higher densities than compressed gas, at pressures below 100 bar, and at higher temperatures than those required for liquid storage. The practical problem is that low temperatures, in the region of 77 K, and pressures up to 100 bar, are still required to achieve high capacities; however, there are also advantages, compared to chemical storage in hydrides, which include rapid sorption kinetics and the low heat of adsorption. The key point is that H_2 storage in nanoporous materials may offer an intermediate solution that provides both high gravimetric and volumetric storage densities at pressures below 100 bar, thus reducing both compression or liquefaction losses and the challenges of handling and distributing H_2 as high pressure (700 bar) gas or cryogenic liquid.

This article covers the fundamentals of H_2 storage in nanoporous materials, and recent work investigating the adsorption behaviour of H_2 at low temperatures and high pressures. We also consider the correlation of gravimetric and volumetric H_2 capacities, enhancing deliverable capacities through the use of flexible materials, machine learning (ML) for predicting storage performance, and assessing the limits of H_2 storage in flexible materials. Other important issues, such as reproducibility testing using interlaboratory exercises and the need for reference materials, are also discussed.

2. Fundamentals

2.1. Gas adsorption in porous materials

The critical point of H_2 is around 33 K and 13 bar, and its boiling point is just over 20 K [17]. Very low temperatures are therefore required to condense hydrogen. These physical properties are due to weak H_2–H_2 interactions, which originate from H_2 molecules having no charge, no dipole moment, a relatively weak quadrupole moment, and a low polarisability. These same characteristics lead to the weak physical interaction of molecular H_2 with surfaces [18–20], but it is nevertheless possible to adsorb fairly large quantities of H_2 at supercritical temperatures, in materials possessing high enough surface areas and pores of proper size.

Various factors affect the adsorption of gases by porous materials, including the strength of the adsorbate–adsorbent interactions, the specific surface area (SSA) of the material, typical pore widths or diameters, and total pore volume. The strength of adsorbate–adsorbent interactions depends on the properties of both the gas and the solid. SSA, meanwhile, defines the extent of the gas–solid interface and thus the quantity of surface sites available for adsorption, per unit mass of material; although the concept breaks down somewhat when pores are sufficiently narrow. At low pressures, the amount of adsorption depends mainly on pore width or diameter. In very narrow pores, the overlapping potentials of opposing pore walls, or of neighbouring framework atoms, lead to stronger solid–fluid interactions compared to open, flat surfaces and therefore to larger amounts of adsorption at relatively low pressure. The saturation uptake of a material, however, at high pressure, tends to scale with the total pore volume up to pore sizes beyond which adsorption is not significant [21].

Adsorption behaviour is typically characterised by the shape of isotherms—plots of uptake against pressure—and varies with temperature. It also correlates with the physical properties of the adsorbate and the nature of the adsorbent. Adsorption at subcritical temperatures differs to supercritical adsorption. Nitrogen is one of the most common adsorbates, due to its widespread use for determining Brunauer–Emmett–Teller (BET) areas, a common approximation of the accessible SSA of a solid. The critical temperature of N_2 is 126 K, while measurements are often performed at its boiling point, 77 K, because of the practical convenience of using liquid N_2 as a cryogen. At such subcritical temperatures, monolayer adsorption can occur on relatively flat or open surfaces, followed by multilayer formation at higher relative pressures, P/P_0, where P is absolute pressure and P_0 is the saturation pressure of the adsorptive. This is the case for non-porous or macroporous materials, and identifying the point at which a statistical monolayer is formed is the principle behind BET surface area determination.

Materials of interest for adsorptive hydrogen storage, however, are usually microporous or mesoporous. Terminology associated with both porous materials and gas adsorption has been defined in widely accepted International Union of Pure and Applied Chemistry (IUPAC) guidelines [22]. Microporous materials are defined as having pore sizes <2 nm; mesoporous materials, between 2 and 50 nm; while the term *nanoporous* refers to any material with a pore size <100 nm [22]. Most porous hydrogen storage materials are therefore nanoporous. In mesoporous materials, at subcritical temperatures, monolayer and multilayer adsorption can occur, followed by capillary condensation, which in most cases gives a characteristic (*Type IV*) isotherm shape with a sudden increase of the amount adsorbed coupled many times with hysteresis between adsorption and desorption isotherms [22–24]. In micropores, however, the adsorption process differs because adsorption only occurs via pore-filling and there is no capillary condensation. This leads to a so-called *Type I* isotherm, which is concave to the pressure axis, with no observable hysteresis. This difference in adsorption behaviour—capillary condensation versus pore filling or else *Type IV* versus *I*—is the historical origin of the otherwise rather arbitrary 2 nm threshold between micropores and mesopores, as defined in the IUPAC guidelines [22].

At supercritical temperatures, even in mesopores, capillary condensation, which is associated with a phase transition from a gas to liquid-like state [23], does not occur. The presence of the surface, however, affects the density of the adsorbate in the pores, to a varying degree, depending on pore size and the strength of the adsorbate–adsorbent interactions. The magnitude of the interaction between an adsorbate and either a surface or a pore of a given size is usually characterised by the heat or enthalpy of adsorption, ΔH, which is typically expressed as *isosteric enthalpy of adsorption*, ΔH_{st}—the differential enthalpy at constant surface coverage or loading [25]. For H_2 on an open carbon surface, for example, ΔH_{st} is approximately 4 kJ mol^{-1} [26], which is rather low considering that the thermal energy at 77 K is around 1 kJ mol^{-1}. ΔH_{st}, however, increases under confinement, while heterogeneities also alter the strength of interaction [27]. Regardless of the chemistry of the adsorbent, however, there is a general trend of increasing enthalpy with decreasing pore size up to the point of molecular sieving [13, 14]. This is a result of the enhanced interaction within small pores due to potential overlap. In some materials, H_2 can also adsorb more strongly on certain types of sites, due to electrostatic interactions [18, 19]. Examples include cations in zeolites [28–30] and open metal sites (OMSs) in MOFs [16, 31]. In these cases, ΔH_{st} for H_2 can exceed 10 kJ mol^{-1} at low loadings.

Isosteric enthalpies are usually determined experimentally by measuring adsorption isotherms at two, or preferably more, closely spaced temperatures, and then applying the Clausius–Clapeyron (CC) equation or van 't Hoff relation [8, 32], while a virial-type analysis is also possible [33, 34]. This results in a plot of ΔH_{st} versus coverage or loading, θ. For H_2, most of the times ΔH_{st} tends to decrease as a function of coverage [14, 25]. This differs to species that may exhibit strong adsorbate–adsorbate interactions at higher coverages. For H_2, the highest values of ΔH_{st}—for strongly interacting sites or the narrowest pores—are found at low coverages. ΔH_{st} at zero coverage can also be calculated by extrapolation or direct calculation. This is, in principle, the energy release due to the adsorption of a single test molecule ($\theta \rightarrow 0$). The magnitude of ΔH_{st} has several practical consequences. Firstly, adsorption can be realised at higher temperatures for higher values of ΔH_{st}. Secondly, more heat is generated upon adsorption when ΔH_{st} is higher, potentially raising heat management issues. Thirdly, from a hydrogen storage perspective, the loading dependence of ΔH_{st} affects the deliverable amount of H_2 at any given pressure, because a high value of ΔH_{st} at low loading, regardless of the value at high loading, will lead to more H_2 being trapped in the material at low pressure, below the delivery pressure of the store [35]. This point is discussed in more detail in section 3.1.2.

Adsorbent heterogeneity due to different surface sites, such as heteroatoms, functional groups, surface defects and so forth, as well as due to different pore sizes within the material also affects ΔH_{st}, as well as isotherm shape. The simplest case is described by the Langmuir model, in which each adsorption site is energetically equivalent and there are no adsorbate–adsorbate interactions. In this case, ΔH_{st} is constant as a function of loading and the isotherm is described mathematically by the Langmuir equation. Most real

adsorbents, however, are not so homogeneous, and the Langmuir equation rarely provides an adequate fit to experimental H_2 adsorption data for nanoporous materials; except perhaps over a limited pressure range.

2.2. Intermolecular interactions

Physical adsorption is generally based on van der Waals interactions, which include long-range attractive forces, between fluctuating, induced or permanent electric moments, but also short-range strong repulsive forces, due to the interaction of overlapping atomic or molecular orbitals (Pauli's exclusion principle) [36, 37]. London dispersion forces are due to electron density fluctuations within atoms, which induce electrical moments in neighbouring atoms and thus attraction [38, 39]. The potential energy of such attractive (negative) interactions between two atoms is given by [40],

$$\varepsilon_{\mathrm{d}}(r) = -A_1 r^{-6} - A_2 r^{-8} - A_3 r^{-10} \cong -A r^{-6} \tag{1}$$

where r is the distance between the centres of the atoms and A_1 (=A), A_2, A_3 are the dispersion constants for instantaneous dipole–dipole, dipole–quadrupole and quadrupole–quadrupole interactions, respectively; the r^{-8} and r^{-10} terms are usually negligible. Short range repulsion (positive) potential energy, meanwhile, can be described by [41],

$$\varepsilon_{\mathrm{R}}(r) = B r^{-m} \tag{2}$$

where B is an empirical constant and m is usually set to 12. The total potential energy between two atoms as a function of their distance can then be approximated by the Lennard-Jones (LJ) expression [42],

$$\varepsilon_{\mathrm{LJ}}(r) = \varepsilon_{\mathrm{d}}(r) + \varepsilon_{\mathrm{R}}(r) = -A r^{-6} + B r^{-12} \tag{3}$$

which has the general shape shown in figure 1(a). This can be recast in a more commonly used form after considering a van der Waals-type diameter, σ, with $\varepsilon_{\mathrm{LJ}}(\sigma) = 0$ and an interatomic distance, r_0, where the interaction is strongest (i.e. the energy, ε_0, is at a minimum and thus $\mathrm{d}\varepsilon_{\mathrm{LJ}}(r)/\mathrm{d}r|_{r_0} = 0$). Then,

$$\varepsilon_{\mathrm{LJ}}(r) = -4\varepsilon_0 \left[(\sigma/r)^{-6} + (\sigma/r)^{-12} \right] \tag{4}$$

where $\varepsilon_0 = \varepsilon_{\mathrm{LJ}}(r_0) = -(A/4)\sigma^{-6}$ and $\sigma = -\sqrt[6]{B/A}$ ($r_0 = \sqrt[6]{2B/A} = \sqrt[6]{2}\sigma$).

For two different atoms, i and j, the Lorentz–Berthelot mixing rules can be used, giving $\sigma_{ij} = {}^1/_2(\sigma_i + \sigma_j)$, while $\varepsilon_{ij} = \sqrt{\varepsilon_i \varepsilon_j}$. The dispersion constant A_{ij} for the atoms is directly related to their properties, for instance, through the Kirkwood–Müller relationship [43, 44],

$$A_{ij} = \frac{6mc^2 \alpha_i \alpha_j}{(\alpha_i/\chi_i) + (\alpha_j/\chi_j)} \tag{5}$$

where α is polarisability, χ is magnetic susceptibility, m is electron mass and c is the speed of light. As an example, the α and χ values for H_2 are 0.79×10^{-24} cm^3 and 4.0×10^{-4} cm^3, respectively, while those for N_2 are 1.76×10^{-24} cm^3 and 12.0×10^{-4} cm^3 [45]. The effect of these different adsorbate properties can be seen in the different calculated potentials for H_2 and N_2 in figure 1(a).

The LJ expression is a 'generic' potential and is thus not necessarily limited to atoms; it can in principle be used for any pair of LJ particles (e.g. figure 1 pertains to H_2 and N_2 spherical molecular models). For instance, the position-dependent energy landscape, $U_{\mathrm{LJ}}(r)$, that a molecule i experiences when close to an open surface, or inside a porous framework comprising j atoms, can be presented as the following summation of all the pairwise LJ potentials,

$$U_{\mathrm{LJ}}(r) = -4\varepsilon_0 \sum_j \left[(\sigma_{ij}/r_{ij})^{-6} + (\sigma_{ij}/r_{ij})^{-12} \right]. \tag{6}$$

For homogeneous flat surfaces the gas-solid interaction potential is more or less similar to the pairwise interaction curve of figure 1(a). The variable in this case, however, is the distance from the surface, z. Upon confinement in pores, such as slits and cylinders, the interaction of neighbouring atoms of the solid sum up in a constructive manner and produce much deeper potential wells compared to the open surface, as shown in figure 1(b). In the case of simple pore models (e.g. slit-shaped or cylindrical pores), the energy landscape can be easily described, as shown in figures 1(b) and (c). Confinement of a gas molecule, however, in a 3D porous solid—for instance, a zeolite or MOF—is far more complicated, as the energy landscape varies in the x, y and z directions, as shown in figure 1(d) for the case of the MOF, HKUST-1.

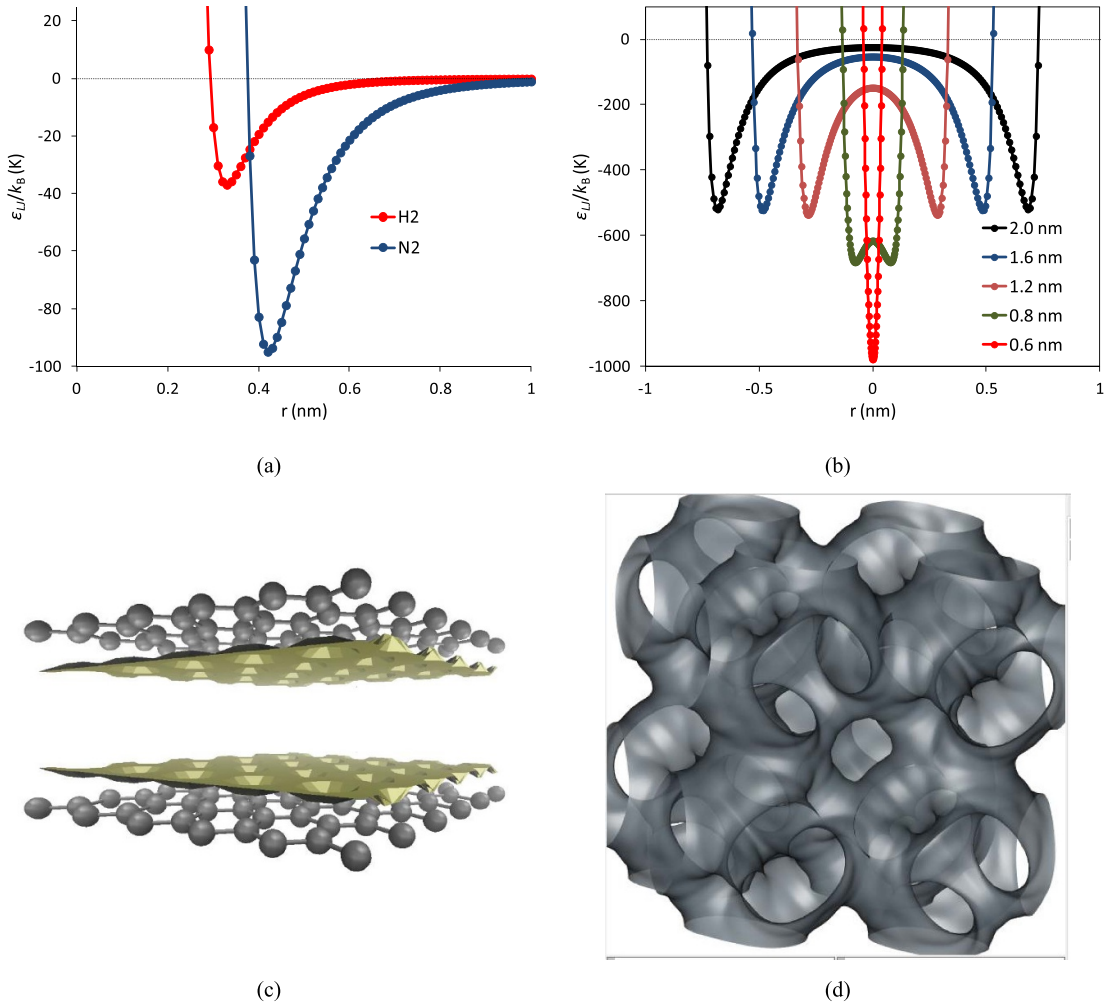

Figure 1. (a) LJ potential energy between two molecules (H_2 or N_2) versus their distance, (b) position dependent potential energy of a single H_2 molecule confined in carbon slit pores of varying width ($z = 0$ is the centre of the pore), (c) LJ zero potential isosurface ($U_{LJ} = 0$) for H_2 in a slit pore with graphene walls. Calculations are based on the visualisation method of [46]. (d) H_2 zero potential isosurface in a typical MOF (HKUST-1). Constructed with i-RASPA visualisation software [47].

For the case of H_2 the interactions become more complicated as the adsorption temperature is reduced since it is a very light gas and therefore has a considerable de Broglie wavelength. For this reason, nuclear quantum effects are expected to contribute significantly to the adsorption process at temperatures below 100 K. For such processes, the quadratic term of the Feynman–Hibbs (FH) effective potential can be used [48], in order to 'smear out' the deepest part of the classical potential curve,

$$U_{\text{all}}^{ij} = U_{\text{LJ}} + \left(\frac{\beta\hbar^2}{24\mu_{\text{m}}}\right)\nabla^2\left(U_{\text{LJ}}\right) \tag{7}$$

where $\hbar = h/2\pi$, h is the Planck constant, $\beta = (kT)^{-1}$ and μ_{m} is the reduced mass, given by,

$$\mu_{\text{m}} = \left(\frac{1}{m_i} + \frac{1}{m_j}\right)^{-1} \tag{8}$$

where m_i is the mass of atom i. The FH expression adequately describes the quantum spreading of H_2 molecules when $\lambda^* = \left(2\pi\beta\hbar^2/m\sigma_{H_2}{}^2\right)^{1/2} \leqslant 0.5$. Here λ^* is the reduced de Broglie wavelength, and m the mass of H_2. The reduced thermal wavelength λ^* at temperature T is given by the expression: $4.17/\sqrt{T}$ and its numerical value at 77 K is 0.47. At lower temperatures, quantum effects become increasingly important and more elaborate approaches, such as the path integral formalism, are required to describe H_2 interactions [49].

2.3. H_2 adsorption at subcritical temperatures

As discussed above, the low molecular mass of H_2 and its weak intermolecular potential result in fascinating properties at cryogenic temperatures of the adsorbed, liquid, and solid phases, comparable only with He. Similarly to other gases below their critical points (e.g. N_2 at 77 K or argon at 87 K) adsorption of H_2 at subcritical temperatures (<33 K) is usually associated, depending on the pore structure and morphology, with processes such as pore-filling and capillary condensation that are not observed at supercritical temperatures. However, in addition to this typical behaviour, H_2 adsorbed at subcritical temperatures, near its boiling point (20.3 K), exhibits unique quantum properties that must be considered for the study of adsorption at such conditions, as well as for the design of cryo-storage systems.

One example that depends on adsorption potential and pore size is the difference in kinetics and adsorption energy upon isotopic (H_2/D_2) exchange. The small difference in mass between the two isotopes (equations (7) and (8)) can lead to quantum sieving which may be kinetic in ultra-microporous (<0.7 nm) materials [50, 51] due to the larger de Broglie wavelength of the lighter isotope (D_2 diffuses faster than H_2 in small pores) or enhanced chemical affinity for the heavier isotope on strong adsorption sites, such as OMSs in MOFs [51–54]. Furthermore, the hydrogen molecule, H–H, possesses two possible proton spin state configurations, ortho-hydrogen (parallel, ↑↑) and para-hydrogen (anti-parallel, ↑↓). Because of the symmetry of the wavefunction, para-hydrogen only has even rotational numbers ($J = 0, 2, 4,\ldots$), while ortho-hydrogen only has odd numbers ($J = 1, 3, 5,\ldots$). The lowest rotational state of ortho-hydrogen is $J = 1$, which implies a quadrupole moment, leading to a stronger interaction when it is physisorbed.

At ambient temperature, the para/ortho ratio is 1:3, whereas at near-boiling temperatures (20 K) it is nearly 1:0. If a H_2 molecule is in the presence of a magnetic centre there may be spin interchange, resulting in ortho-para conversion. This conversion has important practical implications due to the large latent heat of conversion of 1.42 kJ mol^{-1} at 20 K, which is higher than the latent heat of vaporisation of 0.89 kJ mol^{-1} at the same temperature [55]. This effect is often neglected, due to the experimental complication of controlling the para-ortho conversion, and the low temperature at which it is observed.

The quantum nature of molecular H_2 can be also observed in the high compressibility of the bulk solid phase due to the absence of multiple electron shells. Applying a pressure of 100 bar to hydrogen in the solid state results in a volume decrease of 5% [56], whereas other solids are barely compressible. Argon, for example, changes its volume by only 0.8% [57]. This large compressibility also occurs in the adsorbed phase of H_2, which can possess a density higher than the bulk at subcritical temperatures and near ambient pressure, due to short H_2–H_2 intermolecular distances.

2.3.1. High density of H_2 inside the pore system

At 77 K, H_2 physisorption is mainly governed by the surface of the solid, with a linear correlation observed between the SSA (area per unit of mass) and the H_2 gravimetric capacity at elevated pressures, as specified by Chahine's rule [58]. An analogous relation for the volumetric H_2 capacity was recently verified experimentally on a series of MOFs [59]. Gravimetric and volumetric uptake can therefore be correlated to the surface area of the adsorbent [59–61], with an average surface H_2 density of 1.9×10^{-2} mg m^{-2}, measured for many MOFs [59]. This surface density is lower than the bulk density of H_2, and can be understood as the number of H_2 molecules per unit area, equivalent to an intermolecular (H_2–H_2) distance of 4.74 Å at 77 K. This is larger than the intermolecular distance in the solid (3.76 Å) and liquid (4.05 Å) state. Increasing the adsorbed layer density (or reducing the intermolecular H_2–H_2 distance) is important, as it relates directly to an increase in both volumetric and gravimetric H_2 storage capacity of a material.

Measurements of N_2 adsorption at 77 K are routinely used to assess the monolayer capacity of a material; although using Ar at 87 K is preferable, due to its lack of quadrupole moment, as recommended in the IUPAC guidelines [22]. The monolayer capacity, combined with the cross-sectional area of the probe molecule—the area a single molecule occupies on the surface—can be converted into the SSA. Assuming knowledge of the H_2 cross-sectional area, a subcritical H_2 adsorption experiment (<33 K) can therefore, in principle, be used to assess surface area, while simultaneously measuring the maximum capacity of an adsorbent [62]. Despite its importance, the H_2 cross-sectional area cannot be estimated *a priori*. H_2 molecules exhibit weak intermolecular interactions (∼0.3–0.5 kJ mol^{-1}) [63], while the H_2-surface interaction potential for conventional materials such as carbon or silica is ∼4 kJ mol^{-1} [26]. The density of the adsorbed layer or cross-sectional area at low temperatures therefore depends strongly on the H_2-surface interaction, which will be dictated by both the surface chemistry and morphology of the adsorbent.

Subcritical adsorption of light gases, such as He and H_2, has been studied since the 1940s, with some reports revealing unusually high He and H_2 capacities, compared to other gases such as Ar, N_2 or CO_2, in the first adsorbed layer (monolayer) [65, 66]. In 1956, Steele [67] introduced a phenomenological model using the concept of double-layer adsorption (a bilayer) to explain high He monolayer capacities on carbon. Pace and Siebert [68] reported a large discrepancy between the monolayer capacities on carbon of N_2 at 77 K and

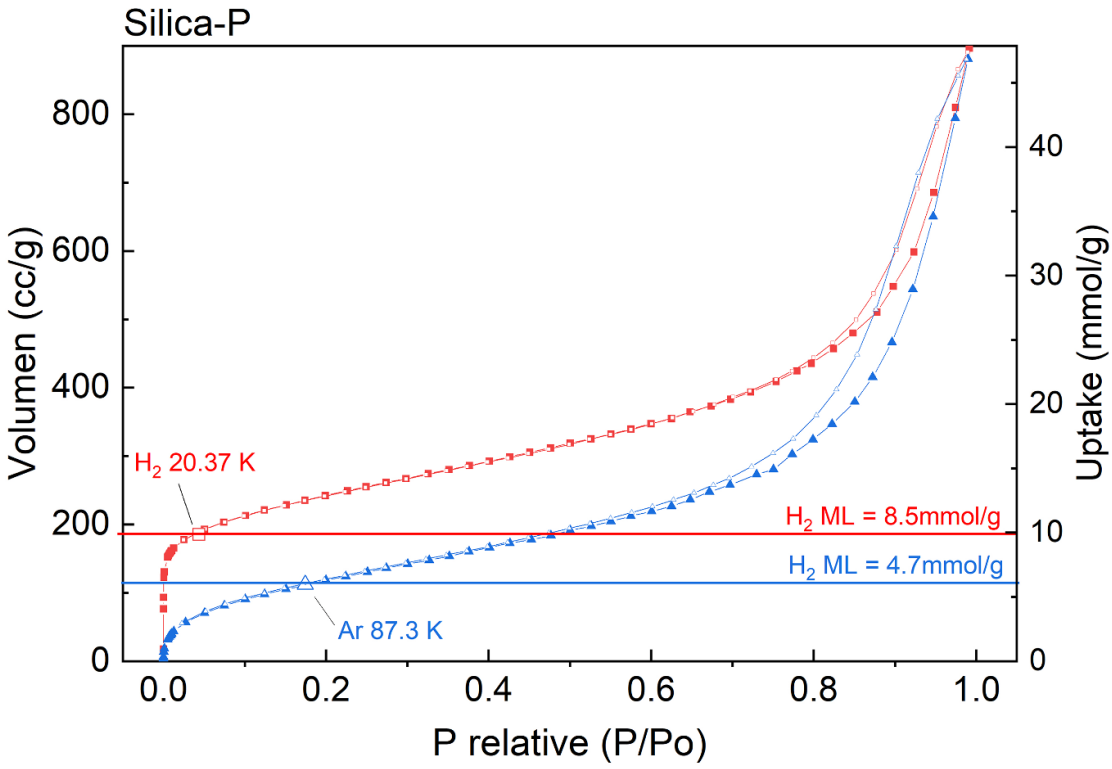

Figure 2. Hydrogen and argon adsorption isotherms of porous silica at boiling temperature, respectively. The monolayer capacities calculated by BET show a difference of almost two times more for H_2, indicating that the two times more molecules cover the same surface [64]. The relative pressure refers to absolute pressure (P) divided by the condensation pressure (P_0).

H_2 at 20 K, suggesting a short intermolecular H_2–H_2 distance (2.95 Å). Such experimental evidence indicated an H_2 adsorbed layer with approximately double the density in graphite-like carbon at 20 K compared to H_2 bulk liquid density. Similar observations have been reported since for H_2 on silica in 1990 [69, 70], 1997 [71] and 2014 [72], for H_2 on carbon in 2004 [73], and for He on zeolites in 1994 [74]. Despite these experiments showing a high adsorption capacity of H_2 (and He) at subcritical temperatures, however, the microscopic nature is still under discussion, with some reports ascribing it to a high-density, monolayer-like H_2 phase, and others assuming the formation of a bilayer.

In recent work, Balderas-Xicohténcatl *et al* [64, 75] studied the density of a single layer of H_2 adsorbed at 20 K on a series of micro-, meso- and non-porous silicas and carbons, as well as the model material KIT-6, a mesoporous silica [76]. High-resolution gas adsorption experiments and inelastic neutron scattering (INS) were used to independently demonstrate layer formation of H_2 with an intermolecular distance of 2.9 Å. Figure 2 shows an example of the comparison of H_2 (20 K) and Ar (87 K) adsorption isotherms for porous silica. The isotherms show that the H_2 BET monolayer capacity is almost double that of Ar for the same surface. The intermolecular H_2–H_2 distance was calculated by comparing the H_2 monolayer capacity and the surface area, and equates to a volumetric density of 201 g cm^{-3}, almost three times the bulk-solid density of H_2 (80.0 g cm^{-3}). These experimental results were supported by path integral Monte Carlo simulations and *ab initio* calculations, including nuclear quantum effects, allowing rationalisation of the high-density phase by the relatively small intermolecular repulsion of the compressed H_2 compared to the surface-adsorbate attraction [64, 75]. This high density, or short intermolecular H_2–H_2 distance, still requires further study, but could potentially be used to increase both volumetric and gravimetric H_2 storage capacities of materials for cryogenic storage systems.

2.3.2. H_2 adsorption near its boiling temperature

Storing H_2 as a liquid in a cryogenic tank has been proposed as an economically viable option for large-scale storage and transport applications, due to the higher energy density and better area/volume ratio of a large tank, which translates into better thermal isolation [77]. Hydrogen liquefaction requires temperatures as low as 33.1 K and a moderate pressure of 12.8 bar. In this context, H_2 adsorption in nanoporous materials near the boiling point could be used to optimise such cryogenic tanks.

One of the first subcritical H_2 adsorption isotherms measured on a MOF, MIL-101, was reported by Streppel *et al* [62]. This material possesses a trimodal pore size distribution, which offered the opportunity to

explore the pore filling effect that occurs at different pressures. Near the condensation pressure, the material is saturated due to the filling of all pores. At this point, the loading reaches an upper limit that defines the saturation capacity of the material. Saturation capacity is technologically relevant since it marks the upper physical limit of an adsorbent-filled tank.

Oh *et al* [78] used an isochoric (constant volume) adsorption experiment to measure the capacity of an empty and a MIL-101 filled sample cell. The isochoric experiment is a direct measurement of the pressure increase with temperature. For the empty tank, the pressure rapidly increases at 20 K, which corresponds to the boiling temperature of H_2. In the presence of the adsorbent, the pressure starts to increase at ca. 40 K over wider temperature range. Hence, H_2 adsorption data near boiling temperature for high-capacity sorbents is also required to assess the potential of achieving the gravimetric and volumetric capacity requirements for on-board H_2 storage systems based on cryo-adsorption.

2.4. Adsorption at high pressure

When measuring gas adsorption at high pressure it is important to distinguish between the excess and absolute adsorbed quantities [15, 74]. Techniques for measuring adsorption isotherms, including both the gravimetric and volumetric/manometric methods, determine *excess adsorption*, which is the amount adsorbed over and above the molar quantity that would be present in the absence of gas–solid interactions. *Absolute adsorption*, meanwhile, is the common term for the total quantity present in the adsorbed phase. An additional term, *total adsorption*, is sometimes used to refer to the sum of adsorbate molecules in the accessible pore volume of the adsorbent. Calculation of absolute uptake from excess uptake, determined from experimentally measured values of pressure, temperature and calibrated volumes, requires knowledge of either the volume occupied by the adsorbate or its density [79]. Experimental determination of the density of H_2 adsorbed in the pores of a material is, however, very difficult [15, 80]. One way to achieve this is to continue to increase the pressure in an experimental isotherm past the point at which adsorption saturates. Provided there is no further adsorption for higher pressure steps and the adsorbate density does not change, the calculated isotherm uptake becomes linear with respect to the bulk gas density, and the slope of this linear portion of the isotherm gives the volume of the adsorbate [81, 82].

As H_2 adsorbs relatively weakly in most porous materials, achieving saturation requires low temperatures, high pressure, or both. Due to difficulties with handling and measuring high pressure H_2 adsorption, low temperatures were first to be investigated. Poirier and Dailly analysed H_2 adsorption measurements on IRMOF-1 [83] and a range of MOFs [84–86] at 50–100 K up to 40 bar, determining densities of the adsorbed H_2 of 0.068 g cm^{-3} and 0.05–0.06 g cm^{-3} respectively. This technique has also been applied to isotherms for other gases, including CO_2 [87–89], and N_2 and CH_4 [89]. In all the H_2 studies mentioned above, pressures less than 100 bar were employed, necessitating temperatures below 100 K in order to reach saturation. At higher temperatures, much higher pressures are needed, as demonstrated by measurements made by Voskuilen *et al* [90] who found that saturation was not reached at ambient temperature for pressures up to 500 bar, for various nanoporous materials, including porous carbons, five different MOFs, and a hyper-crosslinked polymer.

More recently, H_2 adsorption isotherms have been measured on a commercial activated carbon, Filtrasorb 400, at ambient temperature [91]. In order to achieve saturation, measurements were made up to 2000 bar. A typical excess isotherm is shown in figure 3, in which the calculated uptake in wt% is plotted against gas pressure (Plot A). It should be noted that performing adsorption measurements up to this pressure is not routine. It requires H_2 compression, as typical supply cylinder pressures are of the order of 200 bar, as well as the use of specialist high pressure components, including valves, tubes and fittings. Most commercial H_2 adsorption instruments operate up to a maximum pressure of only 200 bar, while the majority of gas adsorption instruments, more generally, for use, for example, for N_2 adsorption, only operate up to ambient pressure (1 bar).

Assuming the adsorbed phase volume, which is often taken as the pore volume of the sample [82, 89, 92], is constant for all points on the isotherm and it is the adsorbate density that changes with uptake, the absolute isotherm can be constructed from the excess isotherm by adding an uptake amount equivalent to the bulk gas density times the adsorbate volume [91]. The absolute isotherm calculated in this way is shown in figure 3, plot B. Again, assuming the adsorbate volume is constant, the density of the adsorbate can be calculated from the absolute mass adsorbed divided by the adsorbate volume, as shown in Plot C.

A linear fit to the last six points of the excess uptake versus gas density isotherm had a regression coefficient of $R = 0.9987$ and gave a volume for the adsorbate of 0.625 cm^3 for the 0.480 g sample. From the maximum uptake of 5.50 wt%, this gives a maximum density of 0.0447 g cm^{-3} for the adsorbed H_2 averaged over the sample. Compared to the H_2 adsorbate density at 50 K on activated carbon of 0.06 g cm^{-3} [93], this ambient temperature adsorbate density is slightly lower, as might be expected for a higher temperature.

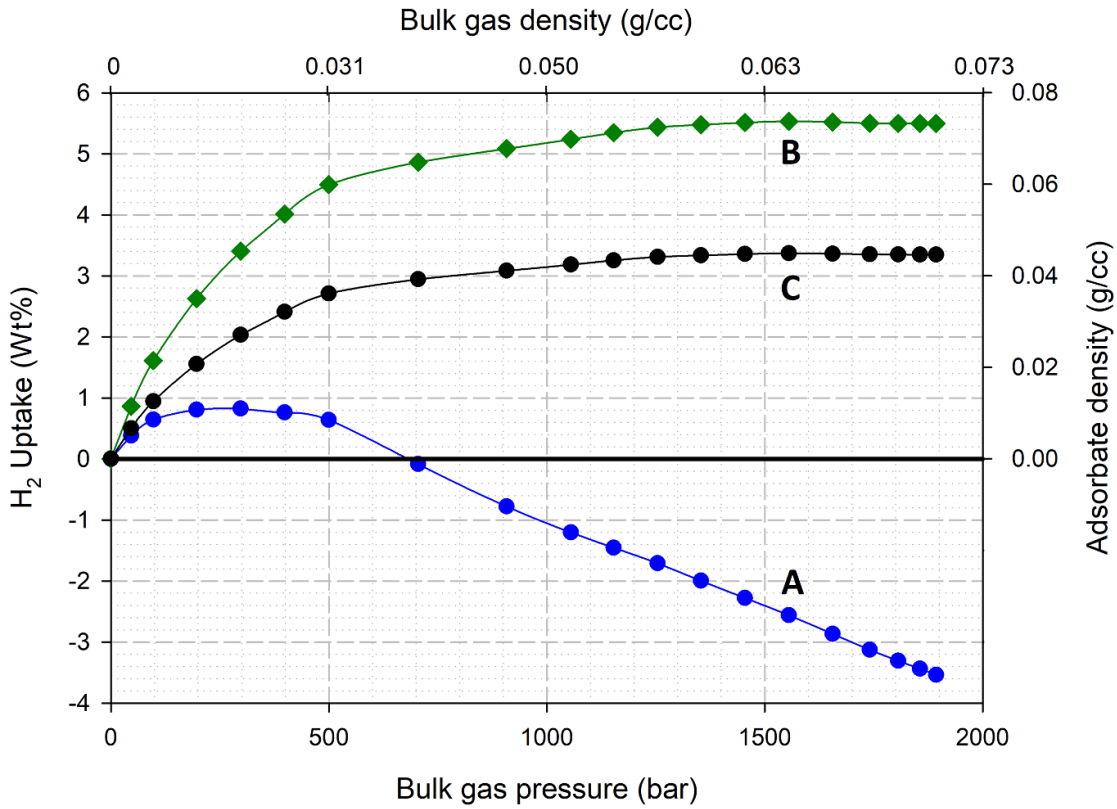

Figure 3. Hydrogen uptake isotherms and adsorbate density at ambient temperature to 2000 bar: plot A, excess isotherm determined from the experimental measurements; B, absolute isotherm calculated from the excess isotherm and the volume of the adsorbate; C, calculated hydrogen adsorbate density. Reproduced from [91], with permission from Springer Nature.

Densities in the range 0.05–0.07 g cm^{-3} have been reported on MOFs at cryogenic temperatures. All these values are lower than the density of liquid H_2 at the boiling point and 1 bar, which is 0.071 g cm^{-3}.

3. Assessing hydrogen storage performance of nanoporous materials

Various measures of the hydrogen storage capabilities of a material have been employed over many years. The primary technique is calculation of the uptake of H_2 as a function of pressure, made by measurements of pressure and temperature over the range of applied pressure. Values for the uptake can be used to determine the gravimetric and, together with knowledge of the volume occupied by the sample, the volumetric, capacities. Another tool for probing hydrogen storage properties is neutron scattering which can yield additional information, such as the location of the adsorbed H_2.

More recently, computational simulations, such as force field and first-principles density functional theory (DFT)-based atomistic modelling, as well as ML-based high throughput screening, are delivering new information and guidance for experimental approaches to new potential materials for hydrogen storage.

Finally, hydrogen storage measurements are only useful if they are accurate and interlaboratory comparison studies indicate that improvements are required, particularly with regard to using consistent terminology and publishing sample preparation details.

3.1. Volumetric and gravimetric capacities

While the amount of hydrogen stored in or on a material is a useful measure of the capacity of a potential hydrogen storage material, the space occupied by the material is also of importance. This is particularly so for practical applications, such as passenger vehicles where there is limited space for fuel tanks. The former capacity, the gravimetric capacity, is usually described in terms of the weight of the hydrogen compared to the weight of the material, whereas the volumetric capacity represents the mass of hydrogen per unit volume occupied by the material.

These capacities and the correlation between the two are discussed in detail below, together with the usable capacity, which is the capacity after practical constraints such as maximum tank pressures and minimum fuel-cell feed pressures are taken into account.

3.1.1. Correlation of volumetric and gravimetric H_2 storage

From a gravimetric perspective, H_2 storage capacity refers to the amount of H_2 adsorbed per unit mass, expressed for instance as g H_2 per g of adsorbent or wt% (g H_2 per 100 g of H_2 loaded adsorbent). At lower temperatures (77 K) and higher pressures (>20 bar), the maximum storage capacity has been found to be directly related to the SSA accessible to H_2 molecules, showing a linear correlation, known as Chahine's rule [58]. This results in 1 wt% H_2 uptake per 500 m^2 g^{-1} of BET area at 77 K. Most of the early development of porous materials for H_2 storage focused on optimising surface area, with the highest excess gravimetric H_2 adsorption capacity of 9.95 wt% measured at 77 K for a material, NU-100, with a SSA of 6143 m^2 g^{-1} [94]. Porous materials with very high SSAs, however, tend to have large pores, which increases the free volume in their open frameworks and decreases their volumetric H_2 storage capacity. A trade-off between total volumetric and gravimetric H_2 capacity has since been identified [60], indicating that MOFs with the best gravimetric performance will generally exhibit relatively modest volumetric capacities.

Volumetric capacity is a primary consideration when evaluating porous materials for H_2 storage and becomes an issue of increasing importance in applications where economy of space is crucial. For instance in the transport sector, and especially for light-duty vehicles, the volume of the H_2 storage tank will be limited. It is therefore the limiting factor in determining the driving range of a vehicle. Volumetric capacity refers to the amount of H_2 adsorbed per unit volume, as g H_2 l^{-1}, in a volume of the tank filled with adsorbent. For an adsorbent, storage capacity is governed by the accessible surface area for the gas; therefore, volumetric capacity will be determined by the surface area per unit volume, i.e. *volumetric surface area*, rather than the gravimetric SSA. This results in an analogous relation to Chahine's rule, between volumetric uptake and volumetric surface area, which was recently verified with experimental data using the packing density and the single crystal density of MOFs [59]. In the same paper, a phenomenological model was developed, based on experimental data that show a direct correlation between volumetric and gravimetric uptake. This suggests that only increasing SSA will not produce a significant increase in the volumetric capacity.

To increase the available volumetric surface area, interpenetrated MOFs have been investigated. *Interpenetration*, meaning the intergrowth of two or more frameworks, is often viewed as a problem when trying to synthesise MOFs [97]; however, in certain cases, it has been found to reduce pore volume, thus increasing the volumetric surface area. CFA-7, the interpenetrated network of the MFU-4 family, has been reported to have a volumetric surface area of 2697 m^2 ml^{-1}, while the non-interpenetrated MFU-4*l* possesses a volumetric surface area of only 1670 m^2 ml^{-1}. The absolute volumetric H_2 storage capacity at 77 K therefore increases from 25 g H_2 l^{-1} to 50 g H_2 l^{-1} at 20 bar in MFU-4*l* and CFA-7, respectively [98].

In recent years, although many nanoporous materials, with different pore sizes, structures and SSAs, have been studied for H_2 storage, the packing density of adsorbent beds has often been overlooked. Typically, the single-crystal density based on crystallographic analysis is used to calculate the volumetric capacity of crystalline materials such as MOFs. However, packing density is important for practical applications. Packing density is commonly a factor of two lower than the single-crystal density. Zacharia *et al* [95] showed that by compacting powder samples, packing density can be increased and the specific volume and interparticle voids reduced. In turn, by eliminating the interparticle voids, the surface area per volume will increase and result in higher volumetric H_2 uptake. Balderas-Xicohténcatl *et al* [59] reported a linear relation of the inverse of the packing density versus SSA for different porous materials. As shown in figure 4, the specific volume shows a linear correlation with SSA calculated for many MOFs using the single crystal volume (blue) and the packing volume of the powder (red). In addition, the similar slopes of the plots of both packing and single crystal volume indicate no significant loss of SSA. For the single crystal case, the intercept corresponds to the skeletal volume, while for powders, the intercept corresponds to the skeletal volume plus the interparticle void volume. This gap between the loose powder packing and single crystal densities can be closed by compacting powder to form monoliths or pellets and reducing the interparticle void volume. Two examples, using MIL-101 (green stars) [96] and MOF-177 (black crosses) [95], show that mechanical compaction of powders reduces the specific volume down to the single crystal volume. For the case of MOF-177, compacting the material further results in the loss of surface area by destruction of the pores and the points follow the linear correlation between the single crystal volume and SSA.

Many attempts have been made to increase volumetric capacity by increasing packing density. Pelletised/compacted SNU-70 exhibits the highest H_2 capacity at 77 K and 100 bar of 33 g ml^{-1} [99]. The current record improvement at 298 K is for zeolite-templated carbon/reduced graphene oxide (ZTC/rGO) monoliths, which have been reported by Gabe *et al* [100] to exhibit a volumetric H_2 storage capacity of 11.2 g l^{-1}, increasing ∼8% over pure compression. Using co-ordinatively unsaturated metal sites (or OMSs), which exhibit strong interactions with H_2, also offers a way of increasing volumetric H_2 storage capacity. The adsorption strength of the positive charge density at the metal cation site increases the amount of gas bound at the working temperature. The best performing material was Ni_2(m-dobdc) (m-dobdc^{4-} = 4,6-dioxido-1,3-benzenedicarboxylate), with a record of 12 g H_2 l^{-1} and 0.9 wt% at 25 °C and 100 bar.

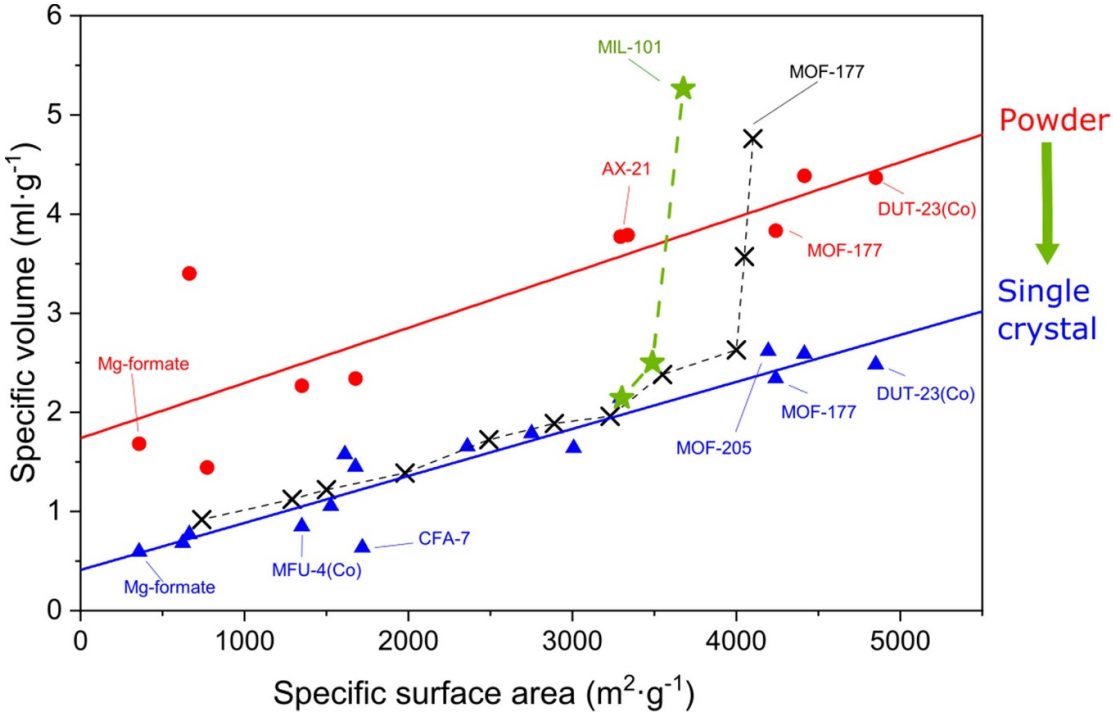

Figure 4. Specific volume using the packing density and single-crystal density (red circles and blue triangles, respectively) as a function of the SSA for porous materials. Data from Zacharia *et al* [95] obtained for a mechanically densified MOF-177 are included as black crosses and data from Blanita *et al* [96] for MIL-101 are included as green stars. The green arrow symbolises the gap for improving the volumetric storage capacity, that can be closed by densification, pelletising or forming monoliths.

However, this approach is limited by the surface density of OMSs in the pores of the framework. Volumetric and gravimetric H_2 capacities are both key factors determining practical system performance in fuel cell vehicles. It is therefore crucial to optimise the volumetric and gravimetric capacities as concurrent parameters.

3.1.2. Usable capacity

Despite the importance of maximum gravimetric and volumetric capacities, usable capacity is another key practical consideration for evaluating adsorbents for H_2 storage. Maximum storage capacities typically reported for adsorbents are defined as the amount adsorbed between vacuum and a maximum storage pressure. From a practical perspective, however, a minimum pressure, in the range 1.5–5 bar, is required to supply a back pressure to the fuel cell stack. Any H_2 adsorbed at pressures below 1.5–5 bar will remain in the material and will therefore be unusable. Usable or deliverable capacity is thus defined as the amount of H_2 released from the adsorbent between full tank conditions and the fuel cell stack back pressure [35].

As mentioned before, surface area, commonly measured by Ar/N_2 adsorption and calculated using the BET method [22], defines the accessible area available for H_2 adsorption (see section 2.1). Storage performance, however, also depends on other adsorbent properties, such as total pore volume, which determines saturation capacities at high pressure, and the magnitude and variation of the gas–solid interaction potential. The latter depends not only on pore size, but also on surface chemistry. The right balance of these properties is required, but deconvoluting the individual contributions is difficult. So, although the search for effective H_2 adsorbents has been ongoing for at least two decades, there are still significant hurdles to developing and deploying nanoporous materials for H_2 storage [16]. Regardless of the impressive maximum gravimetric H_2 capacities reported so far, optimum solutions, in terms of usable or deliverable gravimetric and volumetric capacities, under different temperature and pressure operating conditions, are yet to be achieved.

For a given material, the optimum operating temperature is the temperature at which the maximum usable capacity is obtained. In principle, adsorption on materials exhibiting low ΔH_{st} requires low temperatures/high pressures, while stronger gas-solid interactions and therefore increased ΔH_{st} may allow significant adsorption at higher temperatures and/or lower pressures. In this respect, attempts have been made to develop materials optimised for ΔH_{st}, in order to elevate the operating temperature. The optimum ΔH_{st} was estimated by Bhatia and Myers [101] to be 15–20 kJ mol^{-1}, to achieve H_2 adsorption at ambient temperature at the charging pressure. One way of increasing ΔH_{st} is to introduce strong adsorption centres,

such as undercoordinated metals, to enhance the interaction strength, which will increase the adsorption temperature. However, the surface chemistry is not the only property to be considered; pore size is also important since in small pores, ΔH_{st} increases due to overlap of van der Waals forces [13]. A higher ΔH_{st} increases the temperature at which H_2 can be adsorbed, but it also leads to a weaker temperature dependence of the maximum H_2 uptake at a given pressure [102].

In this respect, Kapelewski *et al* [103], for example, employed a family of structural isomers of M_2(m-dobdc), featuring M^{2+} cation sites with a higher apparent charge density, to increase H_2 binding enthalpies to 8.8–12.3 kJ mol^{-1}. The H_2 capacity was ∼12 g H_2 l^{-1} at 298 K. An even higher H_2 binding enthalpy (−21 kJ mol^{-1}) has been reported by Jaramillo *et al* [104] for the $V_2Cl_{2.8}$(btdd) framework, which contains a high density of exposed vanadium (II) sites. However, even though the total H_2 capacity at ambient temperature was enhanced, both materials showed no increase in usable capacity. To understand this observation, the Langmuir–Freundlich model is applied, in which the usable capacity depends not explicitly on temperature, but on the saturation adsorption and the ratio of the charging pressure to discharge pressure of the tank. The optimum usable capacity can be described as follows:

$$k_{opt} = k\left(p_{max},\, p_{min}, T_{opt}\right) = n_m \frac{\left(\frac{p_{max}}{p_{min}}\right)^{\eta/2} - 1}{\left(\frac{p_{max}}{p_{min}}\right)^{\eta/2} + 1} \tag{9}$$

where k_{opt} is the usable H_2 storage capacity at optimum operating temperature, p_{max} is the maximum permissible pressure of a tank, p_{min} is the required minimum pressure of a fuel cell, n_m is the saturation uptake of a sample in a monolayer, and η is Freundlich exponent.

The parameter η is a temperature-independent material constant. Nevertheless, for several materials with variable enthalpies of adsorption, the following correlation between η and the enthalpy of adsorption is suggested,

$$\eta \approx \frac{-4.63\ \text{kJ mol}^{-1}}{\Delta H_{st}}. \tag{10}$$

Based on the above equations, a lower enthalpy, which decreases the amount of H_2 adsorbed at low pressures, can increase the usable capacity at a particular temperature. In 2012, Schlichtenmayer and Hirscher [13] studied a series of nanoporous materials and found a correlation between the average enthalpy of adsorption and the excess H_2 uptake at 77 K and 20 bar. However, the different enthalpies of adsorption were mainly achieved by varying pore size, rather than by including strong adsorption sites, e.g. OMSs. Since smaller pore size typically coincides with a reduction in SSA, a tendency of lower saturation uptake with increasing enthalpy was observed. In 2016, the same authors evaluated the usable capacity, between 2 and 20 bar, and found a higher optimal operating temperature for materials with higher enthalpies of adsorption [35]. Glante *et al* [105] recently reported a correlation between optimal operating temperature and usable capacity, using the same analysis method. A series of MOFs were investigated and compared to zeolite Ca–A. The optimal operating temperature for most of the MOFs was below 90 K, while for zeolite Ca–A it was ∼120 K. In addition, the usable fraction decreases if one is using a material like zeolite A or a carbon molecular sieve, which have small pore diameters and thus a higher enthalpy of adsorption. This phenomenon has also been confirmed by a computational study by Sun *et al* [106], in which the maximum working capacity was predicted to decrease with increasing optimal temperatures, after screening 64 state points.

Figure 5 summarises the reported data on the correlation of usable fraction and the optimum operating temperature for different porous materials. As the materials have different SSAs (and thus uptakes) usable fraction, defined as the usable capacity at the optimum operating temperature normalised to the uptake at 77 K, has been chosen for comparison. Overall, the higher enthalpy of adsorption associated with small pores or strong adsorption sites increases working temperature, but at the expense of usable capacity. The trade-off between optimal operating temperature and high working capacity is a major roadblock for adsorptive H_2 storage, and needs to be addressed further.

In an ideal scenario, for practical applications, all H_2 uptake/release would occur above the minimum operating pressure of the storage unit, and usable capacity would equal total capacity; although this is usually not the case. Typical rigid materials exhibit classical Langmuir-type absolute adsorption isotherms, where the amount of gas adsorbed increases significantly at relatively low pressure, before reaching a plateau. It is therefore difficult to improve the usable capacity of such adsorbents. To optimise usable capacity, an adsorbent with an 'S-shaped' or 'stepped' adsorption isotherm is desired, in which the adsorbed amount

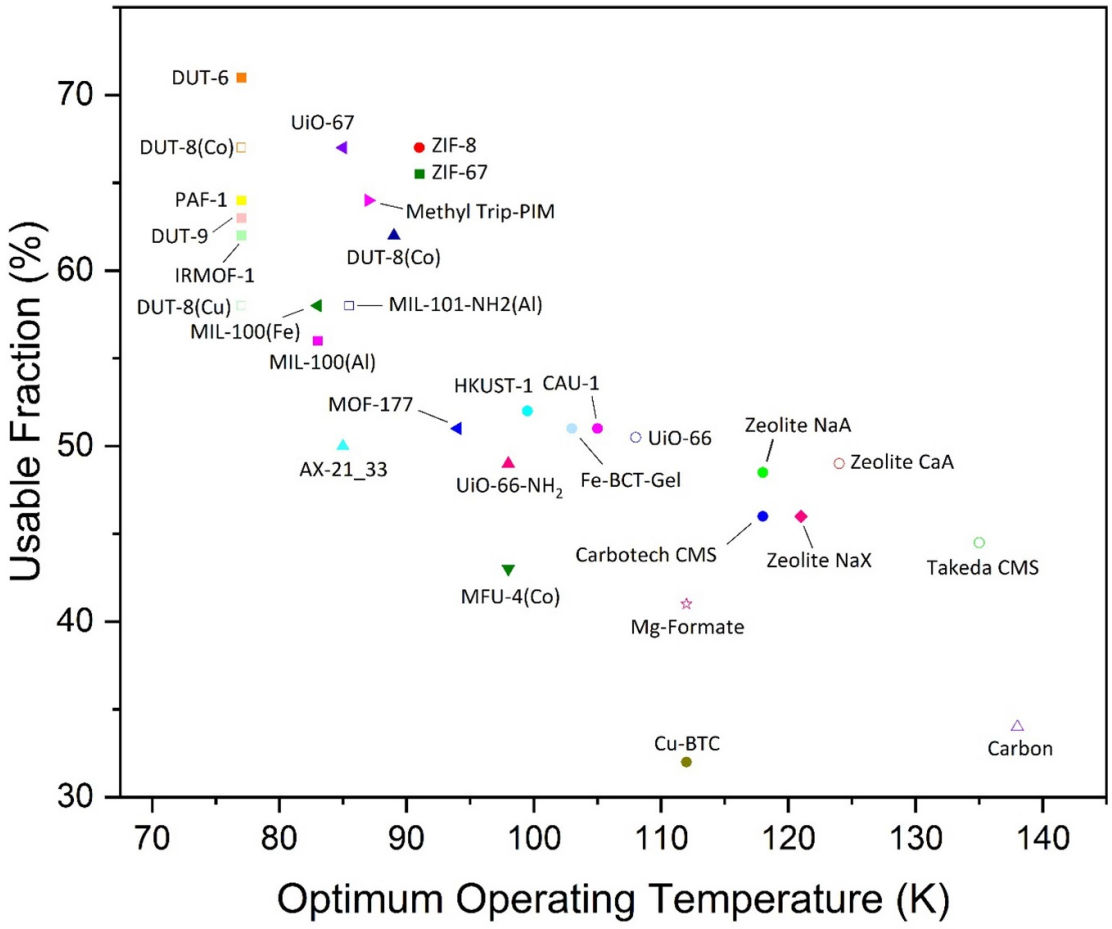

Figure 5. The usable fraction (usable capacity at the optimum operating temperature normalised to the uptake at 77 K and 25 bar) of all materials versus their optimum operating temperature. The materials PAF-1, DUT-6, DUT-8(Cu), DUT-9, and IRMOF-1 are inserted at 77 K, since their optimum temperature could not be identified within the measured temperature range.

would be small at low pressure but would rise sharply just above the delivery pressure. Such stepped isotherms have been reported for the flexible compounds Co(bdq) and Fe(bdq) by Mason *et al* [107] and were attributed to a structural phase transition, enabling higher usable CH_4 storage capacities than rigid adsorbents. Flexible MOFs that exhibit 'gate-opening' behaviour, in which the non-porous structure expands to a porous framework above a certain pressure, have shown hysteretic H_2 adsorption behaviour, resulting in a higher usable capacity. For example MIL-53(Al) exhibited flexibility during H_2 adsorption, revealing an increase in usable capacity [108].

Another option to increase usable capacity is to apply a temperature-pressure swing (TPS) when emptying the tank, by warming the pressure vessel in its depleted state to a higher final temperature. This was first considered by comparing MOF-177 and AX-21 in the pressure range up to 20 bar and at temperatures from 77 K to 125 K and at room temperature [12]. AX-21_33 shows a usable capacity of 3.5 wt% in the case of isothermal operation at 77 K, but 5.6 wt% when the tank is loaded at 77 K and then increased by 40 K during unloading, with a pressure drop from 20 bar to 2 bar. Under the same condition, the usable capacity of MOF-177 increases from 6.1 wt% to 7.4 wt%. As another example, H_2 deliverable capacities under conditions corresponding to charging at 100 bar and 77 K and discharging at 5 bar and 160 K, were evaluated for 14 MOFs [109]. Among the MOFs studied, the gravimetric and volumetric deliverable capacities for NU-125 (49 g l^{-1}, 8.5 wt%), NU-1000 (48 g l^{-1}, 8.3 wt%), and UiO-68-Ant (47 g l^{-1}, 7.8 wt%) are promising for applications in H2 storage and delivery. Moreover, a recent experimental investigation was carried out on NU-1501-Al, which shows one of the highest deliverable hydrogen capacities (14.0 wt%, 46.2 g H_2 l^{-1}) under a combined TPS from 77 K/100 bar to 160 K/5 bar [110].

The challenge for enhancing usable H_2 storage capacity is thus twofold: identify materials whereby H_2 drives structural phase transitions above a certain pressure at a practical temperature but also perform systematic studies of different materials over a range of pressures and temperature. In both fields, computational methods have become an increasingly powerful tool, both for explaining and interpreting experimental results and for guiding experimental work.

3.2. Neutron scattering characterisation of adsorption systems

Understanding the properties of molecular H_2 confined in nanopores is critical to designing and developing new materials and/or processes towards improving current H_2 storage technologies. The microscopic nature of adsorbed molecular H_2 depends on the interaction with the adsorbent surface and the geometry of the pores [72], while confinement can result in phenomena such as phase transitions and hysteresis [111]. Moreover, an adsorbent can also undergo structural changes, due to flexibility, breathing, gate-opening, and so forth, upon gas adsorption or other external stimuli that modify the local environment of the adsorbed H_2 molecules [112].

The aforementioned widely used adsorption methodologies are bulk experimental approaches based on statistically averaged observations. They are key techniques for assessing the performance of hydrogen storage materials but fail to provide direct information on the atomic-molecular level. Scattering and diffraction techniques either in powdered or single crystal samples has proven pivotal in resolving the structure of new crystalline porous sorbents, while synchrotron radiation is in several cases essential due to the low density of the materials. Neutron scattering on the other hand is an ideal tool for the *in-situ* characterisation of H_2 storage materials due to the large cross-section of hydrogen (^{1}H and ^{2}H). This strong neutron scattering power means that atomic positions and motion can easily be detected [113, 114]. However, neutron scattering experiments require a neutron source, typically either a nuclear reactor or a particle accelerator-based spallation source, which are generally large national or international facilities. For interested readers, an earlier discussion of neutron scattering studies of H_2 in nanoporous materials and existing challenges was provided by Broom *et al* [15].

Elastic scattering involves no change in energy of the scattered neutrons and results in diffraction, which provides atomic and/or magnetic structural information, similar to x-ray diffraction (XRD), but with the difference that neutrons interact with atomic nuclei or magnetic moments, rather than the electrons of atoms in a sample. Neutron powder diffraction (NPD) has been successfully applied to understand the structural response of porous frameworks upon gas adsorption, such as MIL-53 [115, 116] and ZIF-7 [117], and to determine adsorbate positions in crystalline porous frameworks [118–120].

INS is especially relevant for H_2 storage in nanoporous materials because it provides a direct spectroscopic probe of the dynamics and local environment of physisorbed H_2, which can be difficult to detect using other techniques. It therefore provides valuable microscopic information on the effects of both surface interactions and confinement. Typically, this characterisation is performed at low temperatures, below the melting point ($\sim$5 K), with H_2 showing quantum properties such as rotational transitions. The lowest possible rotational transition ($J = 1$ to $J = 0$) has a characteristic energy of 14.6 meV, known as the *free rotor transition*. Such a transition is directly visible in an INS experiment and is affected by the local environment of the H_2 molecule. Confinement and adsorption potential symmetry can create a rotational barrier that hinders the free rotor transition [121], and so the hindered rotor transition energies and intensities can be studied to understand the local environment of H_2. Typically, only the molecules in direct contact with the surface are affected by the rotational barrier and the hindering effect can also be used to distinguish the different adsorbed positions in a complex interaction, such as in porous materials with different pore sizes or strong adsorption sites [54]. INS has been used to study molecular H_2 confined within carbon-based materials [72, 122], MOFs [123, 124] and covalent organic frameworks [125]. In combination with structural characterisation methods, such as XRD or NPD, INS can help explain complex adsorbate or adsorbent behaviour, such as flexibility, phase transitions, or quantum effects.

3.3. Computational methods

In parallel to experimental studies, computer simulations and quantum chemical calculations have provided key insights into the hydrogen storage properties of nanoporous materials. Grand canonical Monte Carlo (GCMC) simulations have been widely used to calculate H_2 adsorption capacities at specific temperatures and pressures, while binding sites and energies can be determined using first principles methods, such as electronic DFT and *ab initio* calculations. An earlier discussion of these methods and the challenges involved in performing accurate simulations of H_2 adsorption was provided by Broom *et al* [15], while Allendorf *et al* [16] compared different theoretical methods of calculating H_2 physisorption, including first principles methods, *ab initio* and classical molecular dynamics, and GCMC simulations. The most common theoretical methods used to compute H_2 interactions with adsorbent materials have been summarised in [16], see table 3 therein. In this section, we will now consider the screening of MOFs using ML, and recent work assessing the limits of the deliverable H_2 capacity of flexible materials.

3.3.1. Screening MOFs for H_2 storage using ML

A huge number of nanoporous materials have now been synthesised experimentally, with new materials being reported almost on a daily basis. Some of these materials have been tested for their H_2 storage capacity;

however, due to the expense and time requirements associated with physical experiments, a large proportion of these nanoporous materials are yet to be evaluated experimentally for H_2 storage. Over the past few decades, with advances in computing hardware and software, as well as the development of accurate nanoporous materials databases [126, 127] and efficient ML algorithms [128–130], it has become feasible to run high-throughput computational screening on hundreds of thousands of experimentally synthesised and hypothetical nanoporous materials to assess their suitability for H_2 storage. This approach is much cheaper, and candidate materials with targeted gas storage properties can be identified in a much shorter time scale, and indeed this has led to the discovery of a number of nanoporous materials with excellent gas storage properties.

ML has been used extensively over the last decade to identify materials with specific properties, in a range of different fields. Once an ML model has been constructed, it can provide almost instantaneous predictions for unknown materials. Traditionally, to develop predictive ML models, data from the literature (experimental or theoretical), or data constructed for the purpose of the specific study, are employed. Several ML algorithms are then trained and validated using the data before arriving at the best-performing predictive model. In principle, assuming the ML descriptors are appropriate and the amount of data is sufficient, the ML algorithm can provide predictions of unprecedented accuracy. The development and evaluation of ML descriptors, as well as the accuracy of various ML algorithms for predicting H_2 and other gas adsorption capacities of MOFs, have been studied extensively over the last few years. For H_2 adsorption by MOFs, structural features, such as void fraction, surface area, pore volume, and so forth, have been used as descriptors leading to accurate ML predictions; however, improved performance has been recorded when energy-based descriptors were also employed [129, 131].

In one of the first applications of ML in this area, Borboudakis *et al* [130] constructed a database of 100 experimentally studied MOFs. The metal corners, linkers and functional groups were used as descriptors. A number of different ML algorithms were capable of providing reasonable predictions for the gravimetric capacity of these materials. A combination of ML and molecular simulations was used by Thornton *et al* [132] to screen a library of ∼850 000 materials. Neural networks were trained to predict H_2 adsorption by the materials, using their structural features as descriptors and data generated using GCMC simulations. Candidates with the most promising volumetric working capacities between 100 and 1 bar were identified. More recently, Ahmed and Siegel [128] employed a diverse set of 918 734 MOFs. A sub-set comprising 24 674 MOFs was used to train the ML algorithm, while seven structural features were used as descriptors. The extremely randomised trees algorithm [133] identified more than 8000 MOFs appropriate for pressure swing (PS) and 95 materials for TPS which exceed, within the accuracy of the modelling parameterisation, the gravimetric and volumetric capacities of state-of-the-art materials.

Fanourgakis *et al* [134] recently introduced an iterative self-consistent (SC) approach aimed at rapidly identifying the top-performing materials from a large database of candidates, using a minimum amount of information. The procedure is illustrated in figure 6 and is briefly described as follows: initially a data set is created using information for a small number of materials. These materials could be selected from the database either randomly or using semi-empirical models [60, 132]. An initial ML model is trained on this data and is used for predictions for the remaining materials in the database. A predefined number of ML predicted top-performing MOFs enriches the previous data set which is used, in turn, to construct a second ML model. This procedure is repeated until the predefined number of the predicted top-performing materials has been included in the training data set. Even though the ML predictions are not very accurate during the first iterations, due to the small training set sizes, the majority of materials included in the training data during the next iterations will have high capacities. As a result, successive ML models gradually improve in the region of interest, namely for materials having large capacities. The final ML model provided significantly higher accuracy for materials with large capacities compared to the materials with lower capacities.

Application of the above method to CH_4 adsorption by nanoporous materials [134] showed that more than 70 of the 100 top-performing materials could be identified with only a small amount of information (260–390 MOFs). It is important to mention that, while the previous approach was applied to two databases with sizes differing by more than an order of magnitude (∼5000 MOFs and ∼67 000 covalent organic frameworks (COFs)), the amount of information finally required was similar in both cases. Secondly, the accuracy of the present approach (number of identified top-performing MOFs) is significantly higher than when data sets of similar sizes, containing randomly selected materials, are used instead. For example, in an application of the approach it was found [134] that the SC procedure converged requiring information for only 306 of the 4763 CoRE MOFs. Among them were 76 of the top-100 performing MOFs for CH_4 storage at $P = 5.8$ bar. Instead, the ML model trained using a dataset of 306 randomly selected MOFs was capable of successfully identifying only 50 of the top-100 materials. For constructing efficient ML schemes, aimed at identifying top-performing materials, the proposed iterative procedure can therefore significantly reduce the

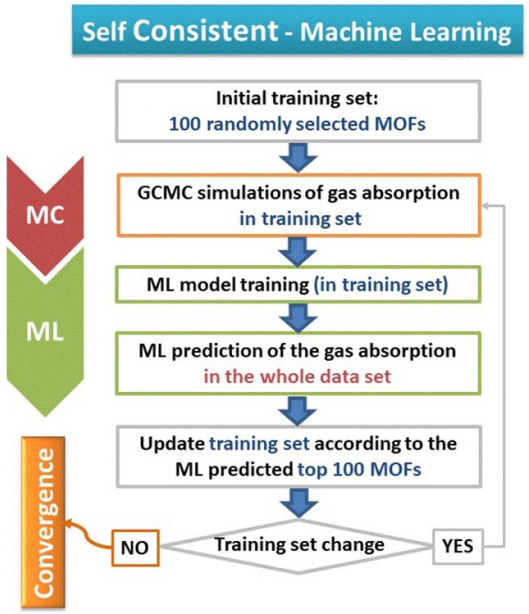

Figure 6. Flowchart of the iterative SC approach used for the identification of the top-performing MOFs for H_2 storage.

number of required simulations. While in the previous application of the SC approach, CH_4 adsorption capacities of materials were computed using GCMC simulations, in principle, experimentally determined adsorption capacities may be used as well.

The same methodology for identifying top-performing materials was employed for H_2 storage. Candidates were selected from a collection of experimentally synthesised and hypothetical MOFs created by Ahmed *et al* [135]. The gravimetric capacity of 98 694 materials for PS between $P = 100$ bar and 5 bar at $T = 77$ K, as well as for TPS between $P = 100$ bar at $T = 77$ K and $P = 5$ bar at $T = 160$ K was also computed by GCMC simulations by the same researchers. Usable capacities, along with several structural features of the MOFs, including void fraction, mass density, and pore limited diameter, were freely distributed by the authors. These results were used to evaluate the approach in terms of accuracy (number of identified top-performing materials) and efficiency (total amount of reference information required). During the application of the SC approach, it was assumed that the adsorption capacities of 100 randomly selected materials are known. Also, after each iteration, the top-100 materials predicted by the ML algorithm were examined. Those not included in the training set were considered during the next iteration. After convergence of the procedure, the results were evaluated by examining the number of materials that were among the top-100 performing ones. In order to avoid any bias from the initial choice of the randomly selected MOFs, the procedure was repeated 100 times and the average results were computed. The final results of the two data sets are shown in figure 7. It is easily seen that under both conditions (PS and TPS) the SC approach was capable of identifying 98 of the top-100 performing materials. On average, information for less than 300 materials was required (298 for PS and 253 for TPS). Since the number of candidates that were examined is ∼3 orders of magnitude larger than the materials for which GCMC simulations were needed (i.e. ∼100 000 versus ∼300) it can be concluded that the proposed SC approach combines both accuracy and efficiency.

3.3.2. Probing limits of deliverable H_2 capacity by modelling intrinsically flexible materials

To achieve technical targets for on-board vehicular storage of H_2, it is important to understand the fundamental limits of deliverable or usable capacity of nanoporous materials, as discussed in section 3.1.2.

The deliverable or usable capacity of a Langmuirian material is maximised by an optimal free energy of adsorption ΔG represented by the orange isotherm in figure 8(a) and is decreased when adsorption is too strong (blue) or too weak (green) [136]. Hydrogen's adsorption enthalpy in porous materials via physisorption is almost exclusively too weak to provide the deliverable capacity required by technical targets (at non-cryogenic temperatures) [137]. Rare exceptions have been demonstrated where materials containing OMSs approach the optimal [104], or even too strong [138], binding energetics; nonetheless, analogues of these materials with a sufficiently high density of such adsorption sites have yet to be discovered [139]. Even if the optimal ΔG of adsorption can be achieved in a high OMS density framework, rigid materials with

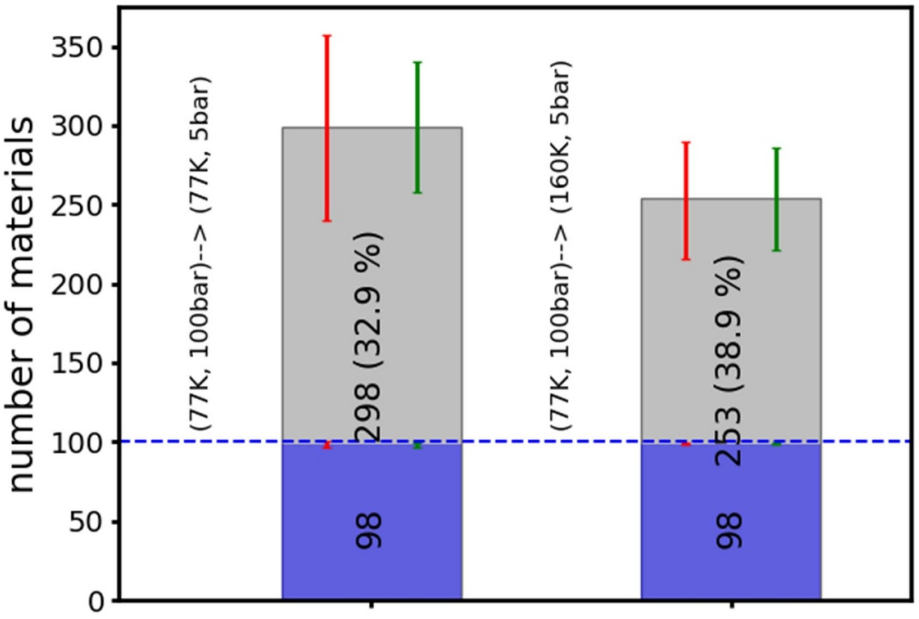

Figure 7. Evaluation of the performance of the SC approach on the identification of performing materials for H_2 storage. In each bar, the number of materials identified as top-performing (blue region) and the total number of materials used for the training of the ML algorithm (grey region) are denoted. The percentage of successfully identified materials over the number of materials for which accurate GCMC simulations were required is given in parentheses. The thermodynamic conditions and the database used are denoted next to each bar. The red error bars at the top of each bar show the minimum and maximum values found during the 100 individual runs, while the green error bars the corresponding standard deviation.

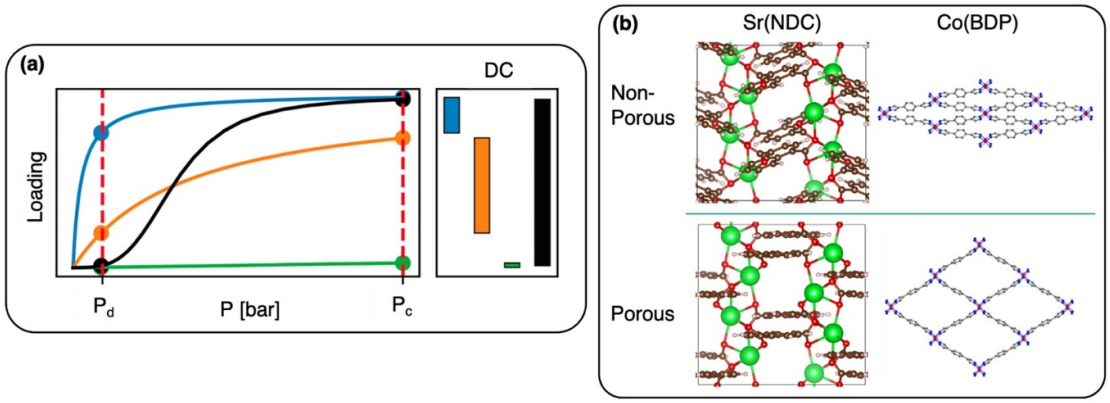

Figure 8. (a) Schematic isotherms of three different Langmuirian materials where deliverable capacity (DC) is maximised from an optimal ΔG of adsorption (orange) or reduced via too strong (blue) or too weak (green) binding of the adsorbate. An intrinsically flexible material with a non-porous (black) isotherm can further maximise deliverable capacity over the optimal Langmuirian material. (b) Examples of intrinsically flexible (left), Sr(NDC) [145], vs extrinsically flexible (right), Co(BDP) [141], MOFs with visualisation of the non-porous and porous states.

Langmuir adsorption behaviour will still suffer a drop in H_2 deliverable capacity (as with any gas) due to unremovable capacity at the discharge pressure, as discussed in section 3.1.2.

One solution is to perform a temperature swing, whereby charging occurs at low temperatures and discharging at high temperatures (also represented by blue and green isotherms, respectively) [140]. Another way to circumvent this problem is to exploit the structural flexibility that many nanoporous materials possess, which can be either intrinsic flexibility (e.g. linker rotation/vibration, see figure 8(b) left) or extrinsic flexibility (e.g. 'breathing' behaviour, see figure 8(b) right) or both. Extrinsically flexible nanoporous materials have been shown to deliver H_2 via an S-shaped isotherm through a large volume contraction from an open-pore phase (charged) to a narrow-pore phase (discharged), therefore increasing the H_2 deliverable capacity, represented by the black isotherm in figure 8(a) [141]. However, the weak interactions of H_2 in this non-OMS framework limited such a phase transition at feasible H_2 pressures to cryogenic temperatures; furthermore, such large volume contraction/expansion would also pose a significant challenge in practical applications, as high mechanical stress associated with large volume changes in some of these materials may

affect long-term structural integrity and therefore adsorption capacity after successive cycles of charging/discharging [142]. Significant attention is therefore placed on intrinsically flexible nanoporous materials which do not experience significant volume change after repeated charging/discharging cycles, and can maintain their structural integrity and mechanical stability under realistic operating conditions [143]. Computational modelling and simulation provide significant insights into such materials and elucidate how and when pore geometry, H_2 binding energetics, and host energetics can produce this desirable non-Langmuirian adsorption profile [144].

In large-scale high-throughput screening studies of nanoporous materials, as described in the previous section, a widely used approximation is the rigid structure assumption. This makes such studies feasible, but also biases the results when the adsorbates of interest have size/shape commensurate with the pores of the adsorbent [146]. In reality, many nanoporous materials have some degree of structural flexibility. One of the consequences is that some of the flexible adsorbents with small pores under the rigid structure approximation (e.g. close to or smaller than the kinetic diameter of a target adsorbate) can be nominally non-porous; however, a slightly higher energy open pore configuration could be stabilised by uptake of H_2 molecules at sufficiently high chemical potential, if H_2 adsorption is sufficiently strong in the open state and the penalty for framework distortion to the open state is sufficiently small. Such materials are destined to be missed by these high-throughput screening studies.

To understand the limit of deliverable capacity in intrinsically flexible nanoporous materials, a statistical adsorption model has been developed by Witman *et al* [144]. Taking CH_4 as an example, it was demonstrated that a perfectly designed nanoporous material with intrinsically flexible slit-pores could achieve higher deliverable CH_4 capacity than the best benchmark systems known to date, with little to no total volume change [144]. Inspired by this flexible slit pore model, electronic DFT calculations and GCMC simulations were performed, from which a known MOF (see figure 8(b) left) was identified that validates key features of the statistical adsorption model. It was also demonstrated that the adsorption thermodynamics, including the energy penalty associated with intrinsic adsorbent linker rotation/vibration and adsorbate binding energy, can be isoreticularly tuned by modifying the linker as well as the metal species of an existing intrinsically flexible MOF. While this study was initially focused on CH_4, it is envisaged that the same computational framework can also be used to study H_2 adsorption and estimate the limit of H_2 deliverable capacity in intrinsically flexible nanoporous materials.

The next challenge would be developing efficient computational approaches to identify intrinsically flexible nanoporous materials with the right pore parameters that lead to optimal H_2 deliverable capacity. Ultimately, a large-scale high-throughput screening study, with carefully chosen and physically informed materials descriptors, relies on a better fundamental understanding of the origin of such intrinsic structural flexibility. An alternative and viable approach, however, would be looking into an existing nanoporous materials database [126], which contains 'cleaned' MOF structures of which guest or solvent molecules were removed from the pores, i.e. these MOF structures resemble the porous ('charged') state. Computational geometry optimisations of these MOF structures in the absence of guest/solvent molecules, using DFT, for example, may result in MOF structures that resemble the nonporous ('discharged') state, providing (a) the open-pore to narrow-pore transition is enthalpy driven, and (b) there is no significant kinetic barrier for this transition. Comparing the two MOF structures in different states and taking into account the prerequisites on negligible or small overall volume change, as well as appropriate pore parameters, it may be possible to identify some, if not all, of the intrinsically flexible nanoporous materials that have excellent H_2 deliverable capacity.

To conclude, effort should be made towards rationally designing nanoporous materials analogous to the above flexible slit pore adsorption model, and we call for continued discovery of intrinsically flexible nanoporous materials with high H_2 deliverable capacity, where such materials remain hidden from rigid structure screening studies due to their nominal non- or low-porosity.

3.4. Reproducibility and interlaboratory exercises

Experimental reproducibility has been an issue in hydrogen storage material research, due to the difficulties of accurately characterising the hydrogen storage properties of materials [8, 147]. Problems have mostly affected nanostructured and nanoporous materials, for which it can be challenging to comprehensively characterise samples, particularly in terms of purity. Experimental errors when measuring H_2 sorption can also be particularly severe for low density materials and increase with increasing pressure [79, 148, 149]. Nanoporous materials of interest for H_2 storage, including carbons and MOFs, are almost exclusively low density, and nanoporosity can lead to difficulties in accurately determining sample volume, which is typically required to perform accurate measurements. In light of these difficulties, Broom and Hirscher [150] recently presented measurement and reporting guidelines, aimed at improving reproducibility in hydrogen storage material research.

Table 1. The relative standard deviation for excess gravimetric hydrogen capacity for 2009 [151] and 2019 [154] for measurements at liquid N_2 and ambient temperatures.

Comparison of the relative standard deviation for excess gravimetric capacity measurements on different carbon samples						
	Liquid N_2 temperature			Ambient temperature		
		2019 study			2019 study	
Pressure (bar)	2009 study	Sample 1	Sample 2	2009 study	Sample 1	Sample 2
5	10.5	5.6	2.2	30	26.8	15.5
10	9.5	3.1	1.1	27.4	12.3	11.1
15	11.1	4.3	1.2	26.5	10.0	11.0
25	—	—	—	22.5	8.1	9.3
50	—	—	—	21.5	6.2	7.8

The challenges of obtaining agreement between H_2 sorption measurements made in different laboratories, which are at the heart of the above problems, were demonstrated by a round robin study published in 2009. Zlotea *et al* [151] reported measurements of H_2 adsorption on a porous carbon up to 200 bar, and found large variations between laboratories in the reported gravimetric capacities. A later, 2013 study involving 14 laboratories subsequently reported measurements of hydrogen absorption by a ball-milled MgH_2 sample [152]. Isotherms were measured at 553 and 593 K and both sets of results had a roughly 7% relative standard deviation in the gravimetric capacity at the plateau equilibrium pressure. In 2016, a comparison of measurements of gravimetric excess capacities for two different carbon samples was published, involving four different research groups who each had over 10 years of experience in the hydrogen storage field [153]. This study showed good measurement agreement and described explicit details of sample preparation and calculations used, providing benchmark H_2 adsorption data for the research community. Nevertheless, these studies clearly illustrated the inherent difficulty in achieving agreement between H_2 sorption measurements made in different laboratories.

Subsequently, in 2019, a study with 13 participating laboratories focused on both gravimetric and volumetric H_2 storage capacities [154]. This investigation involved measuring H_2 adsorption by two porous carbon samples, a pelletised and powder material with surface areas of 1270 $m^2\ g^{-1}$ and 2400 $m^2\ g^{-1}$, respectively, at liquid N_2 and ambient temperatures. In an attempt to compare the 2019 results to the 2009 study, the data from the 2009 work was interpolated to a common pressure and the relative standard deviation was calculated based on the data in the supplementary information. Table 1 lists the relative standard deviation of the 2019 and the 2009 [151] studies for the excess gravimetric capacities at various pressures. It is important to note that data in table 1 represents measurements of different carbon materials, and therefore different magnitudes of excess adsorption. There is also a difference in the methodology for the statistical analysis of the two studies; the 2019 study includes all the reported data, while some outlying data are removed from the analysis from the 2009 work. At both liquid N_2 and ambient temperatures, the relative standard deviation for Sample 1 and 2 in the 2019 study are roughly 50% lower than that of the 2009 data.

In addition to reporting gravimetric capacities for porous carbon samples, the most recent study highlighted the importance of a consistent methodology for determining volumetric H_2 adsorption capacity (see section 3.1.1). Both excess and total volumetric capacities are normalised by a characteristic volume, where the volume can be defined in different ways, for example, crystalline volume, packing volume and envelope volume. A complete discussion of various volumes associated with H_2 storage measurements can be found elsewhere [155–157]. This study used packing volume. One striking finding was the difference in the relative standard deviation of the packing volumes of the pelletised material (4.6%) compared to that of the powder material (27.8%). This uncertainty was reflected in the relative standard deviations of the excess and total volumetric capacities and was attributed to uncertainty in the packing volume measurement and/or real differences in the sample packing densities. This study showed the need for robust and universally accepted definitions, and consistent measurement protocols for reporting volumetric capacities. A material's volumetric capacity is an important performance metric for applications, and measurement protocols must be explicit in order to provide meaningful comparison of a material's hydrogen storage performance.

4. Future developments

The future progress of nanoporous materials for H_2 storage depends on the one side on a large-scale and environmentally-friendly production of affordable materials and on the other side on a reliable and highly

reproducible characterisation of materials properties. The production of materials from sustainable sources will gain importance in a world with limited resources and reduced energy consumption. New interlaboratory tests on hydrogen adsorption properties over a wide range of temperatures and pressures will be needed to get reliable enthalpies of H_2 adsorption, which are required for designing large storage systems. This brings up the demand of reference materials for validation of high pressure H_2 adsorption measurements on porous materials and special challenges in characterising materials under extreme pressures.

4.1. Sustainable material production

Worldwide population growth has led to increasing demand for food and other basic resources, resulting in the intensification of agricultural and industrial activities, and hence in the amount of generated waste. Global annual production of biomass waste and of municipal solid waste (MSW) are of the order of 140 Gt [158, 159] and over 2.1 Bt (0.74 kg/person/day) [160], respectively. Global waste production is expected to grow to 3.40 billion tonnes by 2050, resulting from more than double population growth over the same period. Waste management is therefore critical, and the availability of rapid, low-cost, and economically feasible methods of recovering by-products and turning them into new sources is of considerable academic and industrial interest. Globally, organic (food and green) waste constitutes 44% of total MSW, followed by paper and cardboard (17%), and plastic (12%) [161]. All these materials can be considered, from a circular economy perspective, as a rich and underutilised renewable source of carbon-based materials.

Biochar, a carbon-rich solid residue (C content from 40% to 90%) formed by the pyrolysis of biomass at moderate temperatures (from 673 K to 873 K), has been attracting growing attention in recent years, due to abundant surface functional groups that can have significant effects on the thermodynamics of heterogeneous reactions occurring at the interface, and the possibility of easily tuning porosity by varying the thermal treatment temperature and duration. The application of biochar-based materials as functional composites in energy storage and conversion field is very promising [162]. Concerning H_2 storage, biochar must be activated using, for example, KOH, $ZnCl_2$ or steam [163] in order to create the microporosity required for H_2 adsorption [164]. The biochar material prepared by Xiao *et al* [165], by pyrolysis at 1073 K for 4 h under N_2 atmosphere and subsequent KOH activation of melaleuca bark, for example, shows a surface area up to 3170 $m^2\ g^{-1}$, a micropore volume up to 0.86 $cm^3\ g^{-1}$, and has a H_2 storage capacity of 4.08 wt% at 77 K and 10 bar. Zhang *et al* [166] prepared microporous carbon with surface area of 3200 $m^2\ g^{-1}$and pore volume of 1.44 $cm^3\ g^{-1}$ via pyrolysis and KOH activation of cornstalks and obtained a maximum H_2 adsorption capacity of 4.4 wt% at 77 K and 40 bar. Biochar was prepared from rice bran pyrolysis at 923 K for 12 h and subsequent activation with KOH, obtaining an activated material with a BET area of 2270 $m^2\ g^{-1}$ and a pore volume of 1.22 $cm^3\ g^{-1}$, able to reversibly store up to 4.2 wt% H_2 in less than 1 min at 77 K and 8 bar (manuscript in preparation). One drawback of these materials is the low H_2 adsorption at room temperature (maximum 0.85 wt%), requiring high pressure (up to 100 bar) [167]. Intercalation with alkaline and alkaline earth metals and decoration with transition metals will be attempted on biochar from cereals and vegetable peels to verify their effect in inducing/improving the absorption performance close to room temperature, potentially making these materials appealing for practical applications.

A rather young field is 'green' synthesis of MOFs by either new routes at room-temperature and in water, avoiding energy demanding solvothermal processes [168], or the use of sustainable precursors based on waste materials [169, 170]. MOFs can also be prepared from waste: polyethylene terephthalate bottles, for example, were used to obtain the acid linker terephthalic acid, that served to prepare MOF-5 and UiO-66(Zr) [171, 172]. This last material showed a SSA of 814 $m^2\ g^{-1}$, micropore volume of 0.28 $cm^3\ g^{-1}$, and adsorb 1.2 wt% H_2 at 77 K and 1 bar (to be compared with 1.5 wt% for the commercial cage).

4.2. New inter-laboratory exercises

The interlaboratory exercises performed to date have focussed on measuring H_2 adsorption capacities at 77 K and ambient temperature. Another important parameter, however, is the enthalpy of adsorption, ΔH_{st}, or the coverage dependent isosteric heat of adsorption, q_{st}, which is a metric for the strength of the adsorbent-adsorbate interaction, often used to assess adsorbent properties and compare materials. ΔH_{st} can be measured directly via calorimetry [25, 173] or indirectly through applying the CC approximation to adsorption isotherms taken at different temperatures. Derivation of the CC approximation requires assumptions that may not hold under experimental conditions e.g. the gas in the bulk phase behaves ideally, and the molar volume of the bulk gas is much greater than the molar volume of the gas in the adsorbed phase. In addition, the CC approximation is based on absolute adsorption while isotherm measurements typically measure excess adsorption. Since absolute adsorption cannot be directly measured experimentally, conversion of excess to absolute is required.

The CC approximation is given by,

$$\ln(P) = -\frac{\Delta H_{st}}{R}\frac{1}{T} + C \tag{11}$$

$$\Delta H_{st} = RT_1T_2\left(\frac{\ln(p_1/p_2)}{T_2 - T_1}\right)_n. \tag{12}$$

The enthalpy of adsorption can be calculated using equation (11) by plotting the natural log of the equilibrium pressure, $\ln(P)$, for a constant coverage, n, as a function of inverse temperature, $1/T$, for various measured isotherms. The enthalpy of adsorption is determined from the slope of the line multiplied by the ideal gas constant, R. The method results in ΔH_{st} as a function of moles adsorbed. Equation (12) is a discretised form of equation (11) that can be used with isotherms measured only at two temperatures. Using either equation requires fitting the experimental data with a model isotherm to determine pressure-temperature pairs corresponding to constant moles adsorbed at each isotherm temperature. Details of how the methods are carried out can be found elsewhere [34, 157].

Several reports in the literature have highlighted discrepancies in calculated enthalpies of adsorption via the CC approximation arising from differences in how the equations are applied and how the experimental data is processed [25, 174]. Examples include: whether the CC equation is corrected for the non-ideality of the gas; if and how the data is converted from excess to absolute sorption and the associating assumptions; which isotherm model is used to fit the data; the number of isotherms included in the analysis; the isotherm temperature range; and finally if each isotherm is fit individually or if a single temperature dependent model is used to fit all the isotherms. These variation in analyses make it inherently challenging to judiciously compare competing materials.

An interlaboratory study for determining the enthalpy of adsorption and the associated range of variability would elucidate if and how, and to what extent, different variables and approaches affects the reported results. The objective would be to develop a consensus protocol that allows researchers to converge on best practices for determining the isosteric heat of adsorption. This will enable the hydrogen storage community to better define and compare adsorbate–adsorbent interaction strengths.

An effective study would require identification of a reference material which is uniform, abundant, stable, with a well-defined activation protocol, and an appropriate and measurable adsorption capacity. The material should be well-characterised and have a limited number of homogeneous adsorption sites. Specific parameters for all experiments would be clear and well-defined, including the degassing procedure, sample size, equilibrium time, and pressure range.

The focus would first be to obtain isothermal adsorption measurements at the most experimentally accessible temperatures, for example, 77 K, 89 K, 273 K, and 303 K. Laboratories with more extensive temperature control capabilities could provide isotherm data at additional temperatures. Each research group would be asked to calculate the enthalpy of adsorption using the method they deem most accurate to characterise the extent of deviation within the reported values. In addition, using their same data, researchers would be asked to calculate the enthalpy of adsorption with a common method to determine if consistent results are achievable for material evaluation across different laboratories. The relative standard deviation of the isosteric heat of adsorption will provide a measure of the sensitivity of the calculation method and how differences in measurements are reflected in the calculated data.

4.3. Reference materials

Reference materials are invaluable for validating measurements of any physical or chemical property. Organisations such as the US National Institute of Standards and Technology (NIST) and the Bundesanstalt für Materialforschung und -prüfung, in Germany, provide reference materials for a vast array of purposes. As discussed above, problems have occurred in hydrogen storage material research due to difficulties in obtaining agreement between high pressure H_2 sorption measurements made on the same material in different laboratories. However, there are currently no reference materials available for H_2 adsorption in nanoporous materials, although a EURAMET project, MefHySto, is seeking to rectify this situation. Reference measurements of high pressure CO_2 and CH_4 adsorption on the NIST reference materials, RM 8852 and RM 8850, respectively, have been published recently [175, 176], but there is a clear need for equivalent work to be performed for H_2 adsorption. RM 8852 is ammonium ZSM-5 zeolite and RM 8850 is zeolite Y. The key point is that the availability of a stable nanoporous material, for which the high pressure H_2 adsorption capacity has been determined reproducibly in different laboratories using different apparatus and techniques, would allow independent researchers and laboratories to test the accuracy of their measurement apparatus and protocols. This is a crucial precursor to performing accurate and reproducible

H_2 adsorption measurements on new materials, and so identification of a suitable reference material would have a significant impact on the field.

4.4. Measurement challenges

A considerable amount of computational and experimental research has been conducted on H_2 storage in nanoporous materials over the last two decades or so, as outlined in this article and elsewhere [13, 15, 16, 21, 31, 155]. However, there are perhaps surprising gaps in our knowledge of H_2 adsorption by different materials over a wide range of temperatures and pressures. This information is of fundamental interest, but the H_2 adsorption behaviour of materials, as a function of temperature and pressure, is also required to accurately model the performance of adsorptive H_2 storage units, particularly under different TPS conditions.

The majority of H_2 adsorption data in the literature has been measured at 77 K, due to the relative ease of performing adsorption experiments at this temperature using liquid N_2. Variable low temperature measurements are far more scarce, as are measurements performed beyond 200 bar, at any temperature. It could be argued that H_2 adsorption beyond 200 bar is of limited technological relevance, as the aim of using adsorption to store H_2 is to lower the upper storage pressure to 100 bar or so. However, this does not mean it is not worthy of further study. For some materials, for example, framework flexibility could lead to changes in adsorption behaviour or adsorbed phase density under different temperature and pressure conditions.

With regard to the challenges of such work, it is important to note the variability and irreproducibility of high pressure H_2 adsorption data. It has proven difficult to achieve good agreement between data measured at a single temperature, 77 K, for various reasons [79, 150], so it seems likely that data measured at variable temperatures could be subject to even greater variation. The practical significance of variable temperature data is the possible need to use TPS conditions for storage units, in order to maximise usable capacity. As noted recently by Humayun and Tomasko [88], there has been only a limited number of experimental studies on the usable capacity of different materials under temperature swing conditions.

Two of the fundamental issues with measuring H_2 adsorption at high pressure and variable temperature are accurately describing the density of high pressure H_2, as a function of temperature and pressure, and the density or volume of a material with pores of molecular dimensions. Small errors in the gas density and the volume or density of the solid can lead to large errors in the calculated excess adsorption isotherms. Practical issues include the challenge of operating high accuracy apparatus with H_2, which can be particularly susceptible to leakage. Leakage must be avoided when making H_2 adsorption measurements [79, 150]. Commercial apparatus for such measurements is not widely available and so measurement systems must be custom built [91]. It is therefore likely that this will remain a rather specialist area. To the best of our knowledge, no instruments for making H_2 adsorption measurements to pressures significantly greater than 200 bar, but at variable low temperatures, have been reported. It is possible that *in-situ* neutron scattering experiments could be used to probe the behaviour of H_2 in nanoporous materials at high pressure and variable low temperatures, but the development of appropriate *in-situ* cells for such work brings its own challenges.

5. Conclusion

This article has addressed several important aspects of the fundamentals of hydrogen storage in nanoporous materials, as well as assessment of the performance of different materials, particularly in terms of usable volumetric and gravimetric capacity. Computational techniques, such as ML, have also been discussed, in the context of searching for new rigid and flexible MOFs, together with other important issues, including sustainable production of sorbents, and the use of interlaboratory exercises and the need for standard reference materials, to help improve the reproducibility of experimental H_2 adsorption data.

Research into the use of adsorption to store H_2 in porous materials has evolved significantly in recent years. Although adsorptive H_2 storage was first reported over 40 years ago, using activated carbons, the emergence of carbon nanotubes as a possible storage medium in the late 1990s and MOFs, in the early 2000s, greatly increased the focus on H_2 adsorption as a possible solution to the hydrogen storage problem, alongside hydrides, which have a far longer history. Much of the earlier strategy and work, however, focussed on maximising gravimetric SSA and thus increasing gravimetric capacities, while performance assessment was carried out mainly by adsorption measurements at 77 K. Although this approach is still reasonable to some extent, there has been a notable shift towards considering alternative working conditions, such as temperature swings and adsorption at higher temperatures, and also assessing additional parameters such as usable capacity and volumetric capacity, which have been discussed extensively in this article. Another significant change in recent years has been the introduction of ML methods to rapidly test the H_2 storage capacity of newly synthesised materials or screen hypothetical structures for new candidates with high H_2

uptake. This has allowed a more strategic approach, compared to simply synthesising a material or several materials in a trial-and-error fashion and testing them for H_2 storage experimentally or using GCMC simulation to estimate H_2 uptakes. Nevertheless, current ML approaches can certainly be improved by considering variable working conditions, for example, pressure-temperature swings or avoiding missing flexible frameworks, by assuming that all structures are rigid.

At the start of this article, different aspects of the adsorption of H_2 by nanoporous materials were discussed, including some of the physics behind intermolecular interactions and the adsorption of H_2 in porous materials at different temperatures and pressures, while densification of the nano-confined adsorbed phase under diverse conditions was also detailed. As noted later, there is much that remains unknown about the behaviour of H_2 in nanoporous materials, under a wider range of temperatures and pressures than is typically studied. Further work in this area may lead to a greater understanding of H_2 adsorption, more generally, and this could take us closer to the ultimate goal, which is the development of affordable hydrogen storage tanks that can satisfy the technical requirements for practical applications, in terms of usable volumetric and gravimetric capacity, refill time, safety and energy consumption.

Data availability statement

All data that support the findings of this study are included within the article (and any supplementary files).

Acknowledgments

This paper was realised within the framework of the Hydrogen Technology Collaboration Programme (Hydrogen TCP) of the International Energy Agency (IEA) in Task 40 'Energy storage and conversion based on hydrogen'.

RBX and MH kindly acknowledge funding from the EMPIR programme co-financed by the Participating States and from the European Union's Horizon 2020 research and innovation programme (Project Number: 19ENG03).

RBX gratefully acknowledges research funding from the Hydrogen Materials—Advanced Research Consortium (HyMARC), established as part of the Energy Materials Network under the US Department of Energy, Office of Energy Efficiency and Renewable Energy, Hydrogen and Fuel Cell Technologies Office, under Contract Number DE-AC05-00OR22725.

Sandia National Laboratories is a multimission laboratory managed and operated by National Technology and Engineering Solutions of Sandia, LLC, a wholly owned subsidiary of Honeywell International, Inc., for the US Department of Energy's National Nuclear Security Administration under Contract DE-NA-0003525. M W, M A, and V S gratefully acknowledge funding from the US Department of Energy, Office of Energy Efficiency and Renewable Energy, Hydrogen and Fuel Cell Technologies Office, through the Hydrogen Storage Materials Advanced Research Consortium (HyMARC). This paper describes objective technical results and analysis. Any subjective views or opinions that might be expressed in the paper do not necessarily represent the views of the US Department of Energy or the United States Government.

S L acknowledges the use of the Sulis supercomputer through the HPC Midlands+ Consortium and the ARCHER2 supercomputer through membership of the UK's HPC Materials Chemistry Consortium, which are funded by EPSRC Grant Nos. EP/T022108/1 and EP/R029431/1, respectively.

This work was authored in part by the National Renewable Energy Laboratory, operated by Alliance for Sustainable Energy, LLC, for the US Department of Energy (DOE) under Contract No. DE-AC36-08GO28308. Funding provided by Hydrogen Materials—Advanced Research Consortium (HyMARC), established as part of the Energy Materials Network under the US Department of Energy, Office of Energy Efficiency and Renewable Energy, Fuel Cell Technologies Office, under Contract Number DEAC36-08-GO28308. The views expressed in the article do not necessarily represent the views of the DOE or the US Government. The US Government retains and the publisher, by accepting the article for publication, acknowledges that the US Government retains a nonexclusive, paid-up, irrevocable, worldwide license to publish or reproduce the published form of this work, or allow others to do so, for US Government purposes.

C M, D P and M R gratefully acknowledge research funding from Fondazione Cariplo, GHELF project (Gaining Health and Energy from Lombard Agrifood Waste; n° 2019–2152).

ORCID iDs

Linda Zhang https://orcid.org/0000-0003-3841-544X
Mark D Allendorf https://orcid.org/0000-0001-5645-8246

Rafael Balderas-Xicohténcatl https://orcid.org/0000-0002-5514-412X
Darren P Broom https://orcid.org/0000-0002-1328-7376
George S Fanourgakis https://orcid.org/0000-0001-6158-6824
George E Froudakis https://orcid.org/0000-0002-6907-1822
Thomas Gennett https://orcid.org/0000-0003-1259-6588
Katherine E Hurst https://orcid.org/0000-0003-4596-9504
Sanliang Ling https://orcid.org/0000-0003-1574-7476
Chiara Milanese https://orcid.org/0000-0002-3763-6657
Philip A Parilla https://orcid.org/0000-0002-2056-0289
Sarah Shulda https://orcid.org/0000-0001-8946-1249
Vitalie Stavila https://orcid.org/0000-0003-0981-0432
Theodore A Steriotis https://orcid.org/0000-0003-4978-7513
Colin J Webb https://orcid.org/0000-0001-6659-0726
Matthew Witman https://orcid.org/0000-0001-6263-5114
Michael Hirscher https://orcid.org/0000-0002-3143-2119

References

[1] Toyota 2017 Mirai product information (available at: https://ssl.toyota.com/mirai/assets/core/Docs/Mirai%20Specs.pdf)
[2] Zheng J, Liu X, Xu P, Liu P, Zhao Y and Yang J 2012 Development of high pressure gaseous hydrogen storage technologies *Int. J. Hydrog. Energy* **37** 1048–57
[3] Züttel A 2003 Materials for hydrogen storage *Mater. Today* **6** 24–33
[4] Eberle U, Felderhoff M and Schueth F 2009 Chemical and physical solutions for hydrogen storage *Angew. Chem., Int. Ed.* **48** 6608–30
[5] Aceves S M, Espinosa-Loza F, Ledesma-Orozco E, Ross T O, Weisberg A H, Brunner T C and Kircher O 2010 High-density automotive hydrogen storage with cryogenic capable pressure vessels *Int. J. Hydrog. Energy* **35** 1219–26
[6] Moreno-Blanco J, Petitpas G, Espinosa-Loza F, Elizalde-Blancas F, Martinez-Frias J and Aceves S M 2019 The storage performance of automotive cryo-compressed hydrogen vessels *Int. J. Hydrog. Energy* **44** 16841–51
[7] M Hirscher (ed) 2010 *Handbook of Hydrogen Storage: New Materials for Future Energy Storage* (New York: Wiley)
[8] Broom D P 2011 *Hydrogen Storage Materials: The Characterisation of Their Storage Properties* (London: Springer)
[9] Buschow K, Bouten P and Miedema A 1982 Hydrides formed from intermetallic compounds of two transition metals: a special class of ternary alloys *Rep. Prog. Phys.* **45** 937
[10] Jorgensen S W 2011 Hydrogen storage tanks for vehicles: recent progress and current status *Curr. Opin. Solid State Mater. Sci.* **15** 39–43
[11] Langmi H, Walton A, Al-Mamouria M M, Johnson S R, Book D, Speight J D, Edwards P P, Gameson I, Anderson P A and Harris I R 2003 Hydrogen adsorption in zeolites A, X, Y and rho *J. Alloys Compd.* **356** 710–5
[12] Schlichtenmayer M, Streppel B and Hirscher M 2011 Hydrogen physisorption in high SSA microporous materials–a comparison between AX-21_33 and MOF-177 at cryogenic conditions *Int. J. Hydrog. Energy* **36** 586–91
[13] Schlichtenmayer M and Hirscher M 2012 Nanosponges for hydrogen storage *J. Mater. Chem.* **22** 10134–43
[14] Tedds S, Walton A, Broom D P and Book D 2011 Characterisation of porous hydrogen storage materials: carbons, zeolites, MOFs and PIMs *Faraday Discuss.* **151** 75–94
[15] Broom D P *et al* 2016 Outlook and challenges for hydrogen storage in nanoporous materials *Appl. Phys.* A **122** 151
[16] Allendorf M D *et al* 2018 An assessment of strategies for the development of solid-state adsorbents for vehicular hydrogen storage *Energy Environ. Sci.* **11** 2784–812
[17] Ebeling W, Kraeft W D and Kremp D 1986 Hydrogen plasma—phase diagram and properties *Europhys. News* **17** 52–55
[18] Lochan R C and Head-Gordon M 2006 Computational studies of molecular hydrogen binding affinities: the role of dispersion forces, electrostatics, and orbital interactions *Phys. Chem. Chem. Phys.* **8** 1357–70
[19] Klontzas E, Tylianakis E and Froudakis G E 2011 On the enhancement of molecular hydrogen interactions in nanoporous solids for improved hydrogen storage *J. Phys. Chem. Lett.* **2** 1824–30
[20] Christmann K 1988 Interaction of hydrogen with solid surfaces *Surf. Sci. Rep.* **9** 1–163
[21] Thomas K M 2009 Adsorption and desorption of hydrogen on metal–organic framework materials for storage applications: comparison with other nanoporous materials *Dalton Trans.* **9** 1487–505
[22] Thommes M, Kaneko K, Neimark A V, Olivier J P, Rodriguez-Reinoso F, Rouquerol J and Sing K S W 2015 Physisorption of gases, with special reference to the evaluation of surface area and pore size distribution (IUPAC technical report) *Pure Appl. Chem.* **87** 1051–69
[23] Gelb L D, Gubbins K, Radhakrishnan R and Sliwinska-Bartkowiak M 1999 Phase separation in confined systems *Rep. Prog. Phys.* **62** 1573
[24] Thommes M 2010 Physical adsorption characterization of nanoporous materials *Chem. Ing. Technol.* **82** 1059–73
[25] Kloutse A, Zacharia R, Cossement D, Chahine R, Balderas-Xicohténcatl R, Oh H, Streppel B, Schlichtenmayer M and Hirscher M 2015 Isosteric heat of hydrogen adsorption on MOFs: comparison between adsorption calorimetry, sorption isosteric method, and analytical models *Appl. Phys.* A **121** 1417–24
[26] Wang Q and Johnson J K 1998 Hydrogen adsorption on graphite and in carbon slit pores from path integral simulations *Mol. Phys.* **95** 299–309
[27] Gotzias A, Tylianakis E, Froudakis G and Steriotis T 2012 Theoretical study of hydrogen adsorption in oxygen functionalized carbon slit pores *Microporous Mesoporous Mater.* **154** 38–44
[28] van den Berg A W and Areán C O 2008 Materials for hydrogen storage: current research trends and perspectives *Chem. Commun.* **6** 668–81
[29] Garrone E, Bonelli B and Areán C O 2008 Enthalpy–entropy correlation for hydrogen adsorption on zeolites *Chem. Phys. Lett.* **456** 68–70

[30] Palomino G T, Carayol M L and Areán C O 2006 Hydrogen adsorption on magnesium-exchanged zeolites *J. Mater. Chem.* **16** 2884–5
[31] Murray L J, Dincă M and Long J R 2009 Hydrogen storage in metal–organic frameworks *Chem. Soc. Rev.* **38** 1294–314
[32] Rouquerol J, Rouquerol F, Llewellyn P, Maurin G and Sing K S W 2014 *Adsorption by Powders and Porous Solids: Principles, Methodology and Applications* (Amsterdam: Elsevier) pp 467–527
[33] Czepirski L and Jagiełło J 1989 Virial-type thermal equation of gas–solid adsorption *Chem. Eng. Sci.* **44** 797–801
[34] Nuhnen A and Janiak C 2020 A practical guide to calculate the isosteric heat/enthalpy of adsorption via adsorption isotherms in metal–organic frameworks, MOFs *Dalton Trans.* **49** 10295–307
[35] Schlichtenmayer M and Hirscher M 2016 The usable capacity of porous materials for hydrogen storage *Appl. Phys.* A **122** 379
[36] Gregg S J and Sing K S W 1982 *Adsorption, Surface Area and Porosity* 2nd edn (London: Academic)
[37] Margenau H 1939 van der Waals forces *Rev. Mod. Phys.* **11** 1–35
[38] London F 1930 Zur Theorie Und Systematik Der Molekularkräfte *Z. Phys.* **63** 245–79
[39] London F 1930 Über einige Eigenschaften und Anwendungen der Molekularkräfte *Z. Phys. Chem.* B **11** 222–51
[40] Young D M and Crowell A D 1962 *Physical Adsorption of Gases* (London: Butterworths Scientific Publications)
[41] Abrahamson A A 1963 Repulsive interaction potentials between rare-gas atoms. Homonuclear two-center systems *Phys. Rev.* **130** 693
[42] Lennard-Jones J E 1931 Cohesion *Proc. Phys. Soc.* **43** 461
[43] Müller A 1936 The van der Waals potential and the lattice energy of a n-CH_2 chain molecule in a paraffin crystal *Proc. R. Soc.* A **154** 624–39
[44] Kirkwood J G 1932 Polarisierbarkeiten, suszeptibilitaten und van der waalssche krafte der atome mit mehreren elektronen *Phys. Z.* **33** 57
[45] Olney T N, Cann N, Cooper G and Brion C 1997 Absolute scale determination for photoabsorption spectra and the calculation of molecular properties using dipole sum-rules *Chem. Phys.* **223** 59–98
[46] Karozis S, Charalambopoulou G, Steriotis T, Stubos A and Kainourgiakis M 2017 Determining the specific surface area of metal-organic frameworks based on a computational approach *Colloids Surf.* A **526** 14
[47] Dubbeldam D, Calero S and Vlugt T J 2018 iRASPA: GPU-accelerated visualization software for materials scientists *Mol. Simul.* **44** 653–76
[48] Feynman R 1972 *Statistical Mechanics: A Set of Lectures* ed D Pines (New York: W A Benjamin)
[49] Sesé L M 1995 Feynman-Hibbs potentials and path integrals for quantum Lennard-Jones systems: theory and Monte Carlo simulations *Mol. Phys.* **85** 931–47
[50] Beenakker J, Borman V and Krylov S Y 1995 Molecular transport in subnanometer pores: zero-point energy, reduced dimensionality and quantum sieving *Chem. Phys. Lett.* **232** 379–82
[51] Teufel J, Oh H, Hirscher M, Wahiduzzaman M, Zhechkov L, Kuc A, Heine T, Denysenko D and Volkmer D 2013 MFU-4–a metal-organic framework for highly effective H_2/D_2 separation *Adv. Mater.* **25** 635–9
[52] Li W *et al* 2016 Transformation of metal-organic frameworks for molecular sieving membranes *Nat. Commun.* **7** 1–9
[53] Savchenko I, Gu B, Heine T, Jakowski J and Garashchuk S 2017 Nuclear quantum effects on adsorption of H_2 and isotopologues on metal ions *Chem. Phys. Lett.* **670** 64–70
[54] Weinrauch I *et al* 2017 Capture of heavy hydrogen isotopes in a metal-organic framework with active Cu (I) sites *Nat. Commun.* **8** 1–7
[55] Al Ghafri S *et al* 2022 Hydrogen liquefaction: a review of the fundamental physics, engineering practice and future opportunities *Energy Environ. Sci.* **15** 2690–731
[56] Anderson M and Swenson C 1974 Experimental compressions for normal hydrogen and normal deuterium to 25 kbar at 4.2 K *Phys. Rev.* B **10** 5184
[57] Silvera I F 1980 The solid molecular hydrogens in the condensed phase: fundamentals and static properties *Rev. Mod. Phys.* **52** 393
[58] Chahine R and Bose T (International Association for Hydrogen Energy) 1996 Characterization and optimization of adsorbents for hydrogen storage *Hydrogen Energy Progress XI: Proc. 11th World Hydrogen Energy Conf.* vol 2 pp 1259–64
[59] Balderas-Xicohténcatl R, Schlichtenmayer M and Hirscher M 2018 Volumetric hydrogen storage capacity in metal–organic frameworks *Energy Technol.* **6** 578–82
[60] Goldsmith J, Wong-Foy A G, Cafarella M J and Siegel D J 2013 Theoretical limits of hydrogen storage in metal–organic frameworks: opportunities and trade-offs *Chem. Mater.* **25** 3373–82
[61] Gómez-Gualdrón D A, Wang T C, García-Holley P, Sawelewa R M, Argueta E, Snurr R Q, Hupp J T, Yildirim T and Farha O K 2017 Understanding volumetric and gravimetric hydrogen adsorption trade-off in metal–organic frameworks *ACS Appl. Mater. Interfaces* **9** 33419–28
[62] Streppel B and Hirscher M 2011 Bet specific surface area and pore structure of MOFs determined by hydrogen adsorption at 20 K *Phys. Chem. Chem. Phys.* **13** 3220–2
[63] Diep P and Johnson J K 2000 An accurate H_2–H_2 interaction potential from first principles *J. Chem. Phys.* **112** 4465–73
[64] Balderas-Xicohténcatl R 2019 High-density hydrogen monolayer formation and isotope diffusion in porous media *PhD Thesis* (University of Stuttgart Germany) (https://doi.org/10.18419/opus-10792)
[65] Schaeffer W, Smith W and Wendell C 1949 The adsorption of helium on carbon black at liquid helium temperatures *J. Am. Chem. Soc.* **71** 863–7
[66] Singh R P and Band W 1955 The anomalous monolayer adsorption of helium *J. Phys. Chem.* **59** 663–5
[67] Steele W A 1956 Concerning a theory of multilayer adsorption, with particular reference to adsorbed helium *J. Chem. Phys.* **25** 819–23
[68] Pace E and Siebert A 1959 Heat of adsorption of parahydrogen and orthodeuterium on graphon *J. Phys. Chem.* **63** 1398–400
[69] Huber T and Huber C 1990 Adsorption of hydrogen on porous vycor glass *J. Low Temp. Phys.* **80** 315–23
[70] Huber T and Huber C 1990 Vibrational spectroscopy of porous vycor glass: surface hydroxyl perturbations upon adsorption of hydrogen *J. Phys. Chem.* **94** 2505–11
[71] Edler K J, Reynolds P A, Branton P J, Trouw F R and White J W 1997 Structure and dynamics of hydrogen sorption in mesoporous MCM-41 *J. Chem. Soc. Faraday Trans.* **93** 1667–74
[72] Prisk T R, Bryan M and Sokol P E 2014 Diffusive and rotational dynamics of condensed n-H_2 confined in MCM-41 *Phys. Chem. Chem. Phys.* **16** 17960–74
[73] Tanaka H, Kanoh H, El-Merraoui M, Steele W A, Yudasaka M, Iijima S and Kaneko K 2004 Quantum effects on hydrogen adsorption in internal nanospaces of single-wall carbon nanohorns *J. Phys. Chem.* B **108** 17457–65

[74] Setoyama N and Kaneko K 1995 Density of He adsorbed in micropores at 4.2 K *Adsorption* **1** 165–73
[75] Balderas-Xicohténcatl R *et al* 2022 Formation of a super-dense hydrogen monolayer on mesoporous silica *Nat. Chem.* accepted (https://doi.org/10.1038/s41557-022-01019-7)
[76] Kleitz F, Choi S H and Ryoo R 2003 Cubic Ia3d large mesoporous silica: synthesis and replication to platinum nanowires, carbon nanorods and carbon nanotubes *Chem. Commun.* **17** 2136–7
[77] Zohuri B 2019 *Hydrogen Energy: Challenges and Solutions for a Cleaner Future* (Cham: Springer) pp 121–39
[78] Oh H, Lupu D, Blanita G and Hirscher M 2014 Experimental assessment of physical upper limit for hydrogen storage capacity at 20 K in densified MIL-101 monoliths *RSC Adv.* **4** 2648–51
[79] Broom D P and Webb C J 2017 Pitfalls in the characterisation of the hydrogen sorption properties of materials *Int. J. Hydrog. Energy* **42** 29320–43
[80] Sircar S 2001 Measurement of gibbsian surface excess *AlChE J.* **47** 1169–76
[81] Myers A L and Monson P A 2002 Adsorption in porous materials at high pressure: theory and experiment *Langmuir* **18** 10261–73
[82] Myers A L and Monson P A 2014 Physical adsorption of gases: the case for absolute adsorption as the basis for thermodynamic analysis *Adsorption* **20** 591–622
[83] Poirier E and Dailly A 2008 Investigation of the hydrogen state in IRMOF-1 from measurements and modeling of adsorption isotherms at high gas densities *J. Phys. Chem.* C **112** 13047–52
[84] Poirier E and Dailly A 2009 Thermodynamic study of the adsorbed hydrogen phase in Cu-based metal-organic frameworks at cryogenic temperatures *Energy Environ. Sci.* **2** 420–5
[85] Poirier E and Dailly A 2009 On the nature of the adsorbed hydrogen phase in microporous metal–organic frameworks at supercritical temperatures *Langmuir* **25** 12169–76
[86] Poirier E and Dailly A 2009 Thermodynamics of hydrogen adsorption in MOF-177 at low temperatures: measurements and modelling *Nanotechnology* **20** 204006
[87] Pini R 2014 Interpretation of net and excess adsorption isotherms in microporous adsorbents *Microporous Mesoporous Mater.* **187** 40–52
[88] Humayun R and Tomasko D L 2000 High-resolution adsorption isotherms of supercritical carbon dioxide on activated carbon *AlChE J.* **46** 2065–75
[89] Möllmer J, Möller A, Dreisbach F, Gläser R and Staudt R 2011 High pressure adsorption of hydrogen, nitrogen, carbon dioxide and methane on the metal–organic framework HKUST-1 *Microporous Mesoporous Mater.* **138** 140–8
[90] Voskuilen T G, Pourpoint T L and Dailly A M 2012 Hydrogen adsorption on microporous materials at ambient temperatures and pressures up to 50 MPa *Adsorption* **18** 239–49
[91] Naheed L, Lamb K E, Gray E M and Webb C J 2021 Extracting adsorbate information from manometric uptake measurements of hydrogen at high pressure and ambient temperature *Adsorption* **27** 1–11
[92] Sircar S 1999 Gibbsian surface excess for gas adsorption revisited *Ind. Eng. Chem. Res.* **38** 3670–82
[93] Poirier E 2014 Ultimate H_2 and CH_4 adsorption in slit-like carbon nanopores at 298 K: a molecular dynamics study *RSC Adv.* **4** 22848–55
[94] Farha O K, Yazaydın A Ö, Eryazici I, Malliakas C D, Hauser B G, Kanatzidis M G, Nguyen S T, Snurr R Q and Hupp J T 2010 De novo synthesis of a metal–organic framework material featuring ultrahigh surface area and gas storage capacities *Nat. Chem.* **2** 944–8
[95] Zacharia R, Cossement D, Lafi L and Chahine R 2010 Volumetric hydrogen sorption capacity of monoliths prepared by mechanical densification of MOF-177 *J. Mater. Chem.* **20** 2145–51
[96] Blanita G, Coldea I, Misan I and Lupu D 2014 Hydrogen cryo-adsorption by hexagonal prism monoliths of MIL-101 *Int. J. Hydrog. Energy* **39** 17040–6
[97] Jiang H-L, Makal T A and Zhou H-C 2013 Interpenetration control in metal–organic frameworks for functional applications *Coord. Chem. Rev.* **257** 2232–49
[98] Balderas-Xicohténcatl R, Schmieder P, Denysenko D, Volkmer D and Hirscher M 2018 High volumetric hydrogen storage capacity using interpenetrated metal-organic frameworks *Energy Technol.* **6** 510–2
[99] Purewal J, Veenstra M, Tamburello D, Ahmed A, Matzger A J, Wong-Foy A G, Seth S, Liu Y and Siegel D J 2019 Estimation of system-level hydrogen storage for metal-organic frameworks with high volumetric storage density *Int. J. Hydrog. Energy* **44** 15135–45
[100] Gabe A *et al* 2021 High-density monolithic pellets of double-sided graphene fragments based on zeolite-templated carbon *J. Mater. Chem.* A **9** 7503–7
[101] Bhatia S K and Myers A L 2006 Optimum conditions for adsorptive storage *Langmuir* **22** 1688–700
[102] Schmitz B, Müller U, Trukhan N, Schubert M, Férey G and Hirscher M 2008 Heat of adsorption for hydrogen in microporous high-surface-area materials *ChemPhysChem* **9** 2181–4
[103] Kapelewski M T *et al* 2014 M_2(m-dobdc)(M = Mg, Mn, Fe, Co, Ni) metal–organic frameworks exhibiting increased charge density and enhanced H_2 binding at the open metal sites *J. Am. Chem. Soc.* **136** 12119–29
[104] Jaramillo D E, Jiang H Z, Evans H A, Chakraborty R, Furukawa H, Brown C M, Head-Gordon M and Long J R 2021 Ambient-temperature hydrogen storage via vanadium(II)-dihydrogen complexation in a metal–organic framework *J. Am. Chem. Soc.* **143** 6248–56
[105] Glante S, Fischer M and Hartmann M 2021 Investigation of the optimum conditions for adsorptive hydrogen storage *Mergent Mater.* **4** 1295–303
[106] Sun Y *et al* 2021 Fingerprinting diverse nanoporous materials for optimal hydrogen storage conditions using meta-learning *Sci. Adv.* **7** eabg3983
[107] Mason J A *et al* 2015 Methane storage in flexible metal–organic frameworks with intrinsic thermal management *Nature* **527** 357–61
[108] Mota J P, Martins D, Lopes D, Catarino I and Bonfait G G 2017 Structural transitions in the MIL-53 (Al) metal–organic framework upon cryogenic hydrogen adsorption *J. Phys. Chem.* C **121** 24252–63
[109] García-Holley P *et al* 2018 Benchmark study of hydrogen storage in metal–organic frameworks under temperature and pressure swing conditions *ACS Energy Lett.* **3** 748–54
[110] Chen Z *et al* 2020 Balancing volumetric and gravimetric uptake in highly porous materials for clean energy *Science* **368** 297–303
[111] Narehood D, Grube N, Dimeo R, Brown D and Sokol P 2003 Inelastic neutron scattering of H_2 in xerogel *J. Low Temp. Phys.* **132** 223–37

[112] Schneemann A, Bon V, Schwedler I, Senkovska I, Kaskel S and Fischer R A 2014 Flexible metal–organic frameworks *Chem. Soc. Rev.* **43** 6062–96
[113] Chen Y-P, Bashir S and Liu J L 2017 *Nanostructured Materials for Next-Generation Energy Storage and Conversion: Hydrogen Production, Storage, and Utilization* (London: Springer)
[114] Mitchell P C H, Parker S F, Ramirez-Cuesta A J and Tomkinson J 2005 *Vibrational Spectroscopy with Neutrons: With Applications in Chemistry, Biology, Materials Science and Catalysis* vol 3 (Singapore: World Scientific)
[115] Pollock R A, Her J-H, Brown C M, Liu Y and Dailly A 2014 Kinetic trapping of D_2 in MIL-53 (Al) observed using neutron scattering *J. Phys. Chem.* C **118** 18197–206
[116] Kim J Y *et al* 2020 Specific isotope-responsive breathing transition in flexible metal–organic frameworks *J. Am. Chem. Soc.* **142** 13278–82
[117] Klein R A, Shulda S, Parilla P A, Le Magueres P, Richardson R K, Morris W, Brown C M and McGuirk C M 2021 Structural resolution and mechanistic insight into hydrogen adsorption in flexible ZIF-7 *Chem. Sci.* **12** 15620–31
[118] Dinca M, Dailly A, Liu Y, Brown C M, Neumann D A and Long J R 2006 Hydrogen storage in a microporous metal-organic framework with exposed Mn^{2+} coordination sites *J. Am. Chem. Soc.* **128** 16876–83
[119] Peterson V K, Liu Y, Brown C M and Kepert C J 2006 Neutron powder diffraction study of D_2 sorption in Cu_3 (1, 3, 5-benzenetricarboxylate)$_2$ *J. Am. Chem. Soc.* **128** 15578–9
[120] Yildirim T and Hartman M 2005 Direct observation of hydrogen adsorption sites and nanocage formation in metal-organic frameworks *Phys. Rev. Lett.* **95** 215504
[121] Requena A, Peña R and Serna A 1982 Perturbation for a rigid rotator in an electric field *Int. J. Quantum Chem.* **22** 1263–70
[122] Georgiev P A, Ross D K, Albers P and Ramirez-Cuesta A J 2006 The rotational and translational dynamics of molecular hydrogen physisorbed in activated carbon: a direct probe of microporosity and hydrogen storage performance *Carbon* **44** 2724–38
[123] Rowsell J L C, Eckert J and Yaghi O M 2005 Characterization of H_2 binding sites in prototypical metal-organic frameworks by inelastic neutron scattering *J. Am. Chem. Soc.* **127** 14904–10
[124] Liu Y, Brown C, Neumann D, Peterson V and Kepert C 2007 Inelastic neutron scattering of H_2 adsorbed in HKUST-1 *J. Alloys Compd.* **446** 385–8
[125] Pham T, Forrest K A, Mostrom M, Hunt J R, Furukawa H, Eckert J and Space B 2017 The rotational dynamics of H_2 adsorbed in covalent organic frameworks *Phys. Chem. Chem. Phys.* **19** 13075–82
[126] Chung Y G *et al* 2019 Advances, updates, and analytics for the computation-ready, experimental metal–organic framework database: core MOF 2019 *J. Chem. Eng. Data* **64** 5985–98
[127] Moghadam P Z, Li A, Wiggin S B, Tao A, Maloney A G, Wood P A, Ward S C and Fairen-Jimenez D 2017 Development of a Cambridge Structural Database subset: a collection of metal–organic frameworks for past, present, and future *Chem. Mater.* **29** 2618–25
[128] Ahmed A and Siegel D J 2021 Predicting hydrogen storage in MOFs via machine learning *Patterns* **2** 100291
[129] Bucior B J, Bobbitt N S, Islamoglu T, Goswami S, Gopalan A, Yildirim T, Farha O K, Bagheri N and Snurr R Q 2019 Energy-based descriptors to rapidly predict hydrogen storage in metal–organic frameworks *Mol. Syst. Des. Eng.* **4** 162–74
[130] Borboudakis G, Stergiannakos T, Frysali M, Klontzas E, Tsamardinos I and Froudakis G E 2017 Chemically intuited, large-scale screening of MOFs by machine learning techniques *npj Comput. Mater.* **3** 1–7
[131] Fanourgakis G S, Gkagkas K, Tylianakis E and Froudakis G 2020 A generic machine learning algorithm for the prediction of gas adsorption in nanoporous materials *J. Phys. Chem.* C **124** 7117–26
[132] Thornton A W *et al* 2017 Materials genome in action: identifying the performance limits of physical hydrogen storage *Chem. Mater.* **29** 2844–54
[133] Geurts P, Ernst D and Wehenkel L 2006 Extremely randomized trees *Mach. Learn.* **63** 3–42
[134] Fanourgakis G S, Gkagkas K, Tylianakis E and Froudakis G 2020 Fast screening of large databases for top performing nanomaterials using a self-consistent, machine learning based approach *J. Phys. Chem.* C **124** 19639–48
[135] Ahmed A, Seth S, Purewal J, Wong-Foy A G, Veenstra M, Matzger A J and Siegel D J 2019 Exceptional hydrogen storage achieved by screening nearly half a million metal-organic frameworks *Nat. Commun.* **10** 1–9
[136] Simon C M *et al* 2015 The materials genome in action: identifying the performance limits for methane storage *Energy Environ. Sci.* **8** 1190–9
[137] Llewellyn P L *et al* 2008 High uptakes of CO_2 and CH_4 in mesoporous metal-organic frameworks MIL-100 and MIL-101 *Langmuir* **24** 7245–50
[138] Denysenko D, Grzywa M, Jelic J, Reuter K and Volkmer D 2014 Scorpionate-type coordination in MFU-4*l* metal–organic frameworks: small-molecule binding and activation upon the thermally activated formation of open metal sites *Angew. Chem., Int. Ed.* **53** 5832–6
[139] Witman M, Ling S, Gladysiak A, Stylianou K C, Smit B, Slater B and Haranczyk M 2017 Rational design of a low-cost, high-performance metal–organic framework for hydrogen storage and carbon capture *J. Phys. Chem.* C **121** 1171–81
[140] Kapelewski M T *et al* 2018 Record high hydrogen storage capacity in the metal–organic framework Ni_2(m-dobdc) at near-ambient temperatures *Chem. Mater.* **30** 8179–89
[141] Choi H J, Dinca M and Long J R 2008 Broadly hysteretic H_2 adsorption in the microporous metal–organic framework Co(1, 4-benzenedipyrazolate) *J. Am. Chem. Soc.* **130** 7848–50
[142] Bon V, Kavoosi N, Senkovska I and Kaskel S 2015 Tolerance of flexible MOFs toward repeated adsorption stress *ACS Appl. Mater. Interfaces* **7** 22292–300
[143] Kitagawa S, Kitaura R and Noro S I 2004 Functional porous coordination polymers *Angew. Chem., Int. Ed.* **43** 2334–75
[144] Witman M, Ling S, Stavila V, Wijeratne P, Furukawa H and Allendorf M D 2020 Design principles for the ultimate gas deliverable capacity material: nonporous to porous deformations without volume change *Mol. Syst. Des. Eng.* **5** 1491–503
[145] Raja D S, Luo J-H, Yeh C-T, Jiang Y-C, Hsu K-F and Lin C-H 2014 Novel alkali and alkaline earth metal coordination polymers based on 1, 4-naphthalenedicarboxylic acid: synthesis, structural characterization and properties *CrystEngComm* **16** 1985–94
[146] Witman M, Ling S, Jawahery S, Boyd P G, Haranczyk M, Slater B and Smit B 2017 The influence of intrinsic framework flexibility on adsorption in nanoporous materials *J. Am. Chem. Soc.* **139** 5547–57
[147] Broom D P and Hirscher M 2016 Irreproducibility in hydrogen storage material research *Energy Environ. Sci.* **9** 3368–80
[148] Blach T and Gray E M 2007 Sieverts apparatus and methodology for accurate determination of hydrogen uptake by light-atom hosts *J. Alloys Compd.* **446** 692–7
[149] Webb C J and Gray E M 2014 Analysis of the uncertainties in gas uptake measurements using the Sieverts method *Int. J. Hydrog. Energy* **39** 366–75

[150] Broom D P and Hirscher M 2021 Improving reproducibility in hydrogen storage material research *ChemPhysChem* **22** 2141–57
[151] Zlotea C, Moretto P and Steriotis T 2009 A round robin characterisation of the hydrogen sorption properties of a carbon based material *Int. J. Hydrog. Energy* **34** 3044–57
[152] Moretto P *et al* 2013 A round robin test exercise on hydrogen absorption/desorption properties of a magnesium hydride based material *Int. J. Hydrog. Energy* **38** 6704–17
[153] Hurst K E, Parilla P A, O'Neill K J and Gennett T 2016 An international multi-laboratory investigation of carbon-based hydrogen sorbent materials *Appl. Phys.* A **122** 42
[154] Hurst K E *et al* 2019 An international laboratory comparison study of volumetric and gravimetric hydrogen adsorption measurements *ChemPhysChem* **20** 1997–2009
[155] Broom D P, Webb C J, Fanourgakis G S, Froudakis G E, Trikalitis P N and Hirscher M 2019 Concepts for improving hydrogen storage in nanoporous materials *Int. J. Hydrog. Energy* **44** 7768–79
[156] Parilla P A, Gross K, Hurst K and Gennett T 2016 Recommended volumetric capacity definitions and protocols for accurate, standardized and unambiguous metrics for hydrogen storage materials *Appl. Phys.* A **122** 201
[157] Gross K J *et al* 2016 *Recommended Best Practices for the Characterization of Storage Properties of Hydrogen Storage Materials* (Golden, CO: EMN-HYMARC)
[158] Tripathi N, Hills C D, Singh R S and Atkinson C J 2019 Biomass waste utilisation in low-carbon products: harnessing a major potential resource *npj Clim. Atmos. Sci.* **2** 1–10
[159] UNEP 2015 Converting waste agricultural biomass into a resource (United Nations Environment Programme Division of Technology, Industry and Economics International Environmental Technology Centre) (available at: www.unep.org/ietc/Portals/136/Publications/Waste%20Management/WasteAgriculturalBiomassEST_Compendium.pdf)
[160] Sharma K D and Jain S 2020 Municipal solid waste generation, composition, and management: the global scenario *Soc. Responsib. J.* **16** 917–48
[161] World Energy Council, World Energy Resources 2016 Summary (available at: www.worldenergy.org/assets/images/imported/2016/10/World-Energy-Resources-Full-report-2016.10.03.pdf)
[162] Liu W-J, Jiang H and Yu H-Q 2019 Emerging applications of biochar-based materials for energy storage and conversion *Energy Environ. Sci.* **12** 1751–79
[163] Liu W-J, Jiang H and Yu H-Q 2015 Development of biochar-based functional materials: toward a sustainable platform carbon material *Chem. Rev.* **115** 12251–85
[164] Züttel A, Sudan P, Mauron P and Wenger P 2004 Model for the hydrogen adsorption on carbon nanostructures *Appl. Phys.* A **78** 941–6
[165] Xiao Y, Dong H, Long C, Zheng M, Lei B, Zhang H and Liu Y 2014 Melaleuca bark based porous carbons for hydrogen storage *Int. J. Hydrog. Energy* **39** 11661–7
[166] Zhang F, Ma H, Chen J, Li G-D, Zhang Y and Chen J-S 2008 Preparation and gas storage of high surface area microporous carbon derived from biomass source cornstalks *Bioresour. Technol.* **99** 4803–8
[167] Sevilla M and Mokaya R 2014 Energy storage applications of activated carbons: supercapacitors and hydrogen storage *Energy Environ. Sci.* **7** 1250–80
[168] Steenhaut T, Hermans S and Filinchuk Y 2020 Green synthesis of a large series of bimetallic MIL-100 (Fe, M) MOFs *New J. Chem.* **44** 3847–55
[169] Crickmore T S, Sana H B, Mitchell H, Clark M and Bradshaw D 2021 Toward sustainable syntheses of Ca-based MOFs *Chem. Commun.* **57** 10592–5
[170] Dyosiba X, Ren J, Musyoka N M, Langmi H W, Mathe M and Onyango M S 2019 Feasibility of varied polyethylene terephthalate wastes as a linker source in metal–organic framework UIO-66 (Zr) synthesis *Ind. Eng. Chem. Res.* **58** 17010–6
[171] Roy P K, Ramanan A and Rajagopal C 2013 Post consumer PET waste as potential feedstock for metal-organic frameworks *Mater. Lett.* **106** 390–2
[172] Dyosiba X, Ren J, Musyoka N M, Langmi H W, Mathe M and Onyango M S 2016 Preparation of value-added metal-organic frameworks (MOFs) using waste PET bottles as source of acid linker *Sustain. Mater. Technol.* **10** 10–13
[173] Sircar S, Mohr R, Ristic C and Rao M 1999 Isosteric heat of adsorption: theory and experiment *J. Phys. Chem.* B **103** 6539–46
[174] Pan H, Ritter J A and Balbuena P B 1998 Examination of the approximations used in determining the isosteric heat of adsorption from the Clausius–Clapeyron equation *Langmuir* **14** 6323–7
[175] Nguyen H G T *et al* 2020 A reference high-pressure CH_4 adsorption isotherm for zeolite Y: results of an interlaboratory study *Adsorption* **26** 1253–66
[176] Nguyen H G T *et al* 2018 A reference high-pressure CO_2 adsorption isotherm for ammonium ZSM-5 zeolite: results of an interlaboratory study *Adsorption* **24** 531–9